Astron. Astrophys. Suppl. Ser: 92, 237-265 (1992)

ASTRONOMY & ASTROPHYSICS
SUPPLEMENT SERIES

Astron. Astrophys. Suppl. Ser. **92,** 237-265 (1992)

The Ulysses solar wind plasma experiment

S. J. Bame[1], D. J. McComas[1], B. L. Barraclough[1], J. L. Phillips[1], K. J. Sofaly[1], J. C. Chavez[2], B. E. Goldstein[3], and R. K. Sakurai[3]

[1] University of California, Los Alamos National Laboratory, Los Alamos, NM 87545, USA
[2] Sandia National Laboratories, Albuquerque, NM 87185, USA
[3] California Institute of Technology, Jet Propulsion Laboratory, Pasadena, CA 91109, USA

Received April 8; accepted July 16, 1991

Abstract. — The Solar Wind Plasma Experiment on Ulysses is accurately characterizing the bulk flow and internal state conditions of the interplanetary plasma in three dimensions on the way out to Jupiter. These observations will continue over the full range of heliocentric distances and heliographic latitudes reached by the probe after its encounter with Jupiter and consequent deflection out of the ecliptic plane. Solar wind electrons and ions are measured simultaneously with independent curved-plate electrostatic analyzers equipped with multiple Channel Electron Multipliers (CEMs). The CEMs are arranged to detect particles at chosen polar angles from the spacecraft spin axis; resolution in spacecraft azimuth is obtained by timing measurements with the spacecraft Sun clock as the spacecraft spins. Electrons with central energies extending from 0.86 eV to 814 eV are detected at seven polar angles and various combinations of azimuth angle to cover the unit sphere comprehensively, so as to enable computation of the pertinent electron velocity distribution parameters. As the average electron flux level changes with heliocentric distance, command control of the CEM counting intervals is used to extend the dynamic range. Ions are detected between 255 eV/q and 34.4 keV/q using appropriate subsets of 16 CEMs at spin angles designed to provide matrices of counts as a function of energy per charge, azimuth angle, and polar angle centered on the average direction of solar-wind flow. Data matrices are obtained every 4 min when the spacecraft is actively transmitting and every 8 min during data store periods. These matrices contain sufficient energy and angle resolution to permit a detailed characterization of the ion velocity distributions, from which ion bulk parameters are derived. As the average ion flux intensity changes with heliocentric distance, the entrance aperture size is periodically optimized by command selection from a set of seven apertures on a disk driven by a stepping motor. Changes in the average solar wind flow direction relative to the Earth-pointing spacecraft spin axis are accommodated by command selection of the proper measurement matrix from a set of 11 matrices. In a separate mode of operation and under favorable conditions, heavy ions of oxygen, silicon, and iron at various charge levels are resolved.

Key words: Sun: solar poles — solar wind: latitudinal variation — interplanetary/heliospheric medium.

1. Scientific objectives.

Ulysses is providing an exciting opportunity to explore and characterize the heliospheric medium from the ecliptic plane to above the solar poles at distances from the Sun extending from 1 AU to 5 AU. Observations made on the way out to Jupiter are extending our knowledge of the interplanetary medium in the ecliptic plane, gained from the Pioneer and Voyager flights, while observations made after Ulysses encounters Jupiter and journeys over the solar poles will be unique. The primary objective of the Ulysses solar wind plasma investigation, SWOOPS (Solar Wind Observations Over the Poles of the Sun), is to investigate and establish bulk flow parameters and internal state conditions of the solar wind as a function of solar latitude. Further important goals include studies of radial gradients of solar wind properties between Earth and Jupiter and investigations of the solar wind interaction with the Jovian magnetosphere. Among the important objectives of the SWOOPS investigation are the following:

- Determine systematic variations in the solar wind bulk flow with solar latitude,
- Examine physical processes important for driving the coronal expansion,
- Investigate variations in the evolution of high speed streams with latitude,
- Investigate changes in the nature of transient disturbances with latitude,

Send offprint requests to: S.J. Bame.

- Determine latitudinal variations in the relative abundance and charge state composition of solar wind minor ions,
- Search for and identify plasma mechanisms regulating the electron heat flux, ion beam relative flow velocities, and the He^{++} to H^{+} ion temperature ratio,
- Survey latitudinal variations in Alfvén wave amplitudes and the relative numbers of tangential and rotational discontinuities,
- Determine coronal hole temperatures at which high speed stream solar wind Fe ionization states are established,
- Estimate the electrostatic potential and electron collision length dependence on latitude,
- Identify local heating mechanisms of solar wind ions,
- Study the interaction of interstellar neutrals with the solar wind,
- Study large amplitude hydromagnetic waves, and
- Evaluate radial and meridional gradients in solar wind electron temperature and anisotropy.

1.1. Global properties of the solar wind.

Much is known about solar wind structure and dynamics in the near-ecliptic region of interplanetary space from plasma measurements made during the past 30 years. Very little is known about physical conditions in the polar regions of the solar corona and solar wind. For example, information concerning the variation with heliographic latitude of so fundamental a flow parameter as the solar wind mass flux is lacking. Similarly, little is known about latitude variations of the energy and momentum fluxes, the internal plasma state, and hydromagnetic wave field. Yet these parameters are important in determining the physical state of the polar corona as well as the size and shape of the heliospheric cavity which separates the Sun from the local interstellar medium. They are also important for understanding: (a) the physical processes dominant in accelerating and modulating energetic charged particles, (b) the interaction between the Sun and the neutral component of the local interstellar medium, (c) the nature of the interplanetary scintillation of radio sources, and (d) the evolution of cometary bodies and dust grains orbiting the Sun in interplanetary space. A prime objective of the SWOOPS investigation is to fill the present gap in our knowledge of the local solar neighborhood by providing three-dimensional (3D) measurements of the solar wind electrons, and the H, He, and heavier ion components at latitudes ranging from the solar equator to near the solar poles.

1.2. Energetics and acceleration of the solar wind.

A fundamental goal of current research is to understand the physical processes that maintain a hot corona and accelerate coronal plasma into interplanetary space. It has been necessary to draw inferences concerning these processes from observations made far from the Sun and generally in the ecliptic plane, where dynamical processes make it difficult to separate the basic solar wind states from states altered during transit through interplanetary space. Ulysses will make possible studies of the very simplest corona/solar wind regions, such as the expansion from long-lived polar coronal holes in which stream-stream interactions should be absent and in which the magnetic field should have a relatively simple configuration, extending outward nearly radially. Observations of the density, flow speed, electron and ion internal states, the hydromagnetic wave field, and the minor ion composition in the polar solar wind with SWOOPS will provide information relating to the solar wind acceleration that should be applicable to all latitudes including the ecliptic plane.

1.3. Nonlinear MHD disturbances – large scale solar wind structures.

The large scale solar wind structures in the ecliptic are usually high speed and low -speed streams from coronal holes and the equatorward coronal streamer belt. Solar rotation ensures that these flows interact with each other even when the corona is evolving slowly with time. The picture is additionally complicated by coronal mass ejection, CME, events which propel fresh coronal material into the solar wind.

At the present time little is known about how corotating structures and transient disturbances interact with each other and evolve at solar latitudes away from the ecliptic plane. Some evidence suggests that high-speed streams are bounded on all sides by large shears. Knowledge of the 3D shapes of shocks and other transient structures in interplanetary space is needed to gain a global perspective of the flow of energy from energetic coronal events into the heliosphere. Not only is the physics of these flow interactions of interest in its own right, but the global structure of the interactions affects a variety of related disciplines. For example, energetic particles are modulated and/or accelerated by their interaction with both transient-driven and corotating shock disturbances, the heliosphere boundary is buffeted by these disturbances, and the brightness of comets is thought to be enhanced by interactions with shock wave disturbances. The long term observation of these large scale plasma structures away from the ecliptic plane with the SWOOPS experiment will clarify and enhance the knowledge that has been gained with in-ecliptic observations.

1.4. Large-amplitude hydromagnetic waves – small scale solar wind structures.

On a time scale of hours, large amplitude solar wind irregularities are generally collisionless hydromagnetic fluctuations. They may be either propagating waves or plasma variations that are at rest with respect to the solar wind. Many such structures can be identified as Alfvén waves, or tangential or rotational discontinuities. The relation of the amplitudes, polarizations, modes, and spectra of interplanetary fluctuations to the large scale structure of the solar wind is of great interest. Acquisition of a global perspective of the evolution of large amplitude hydromagnetic waves and turbulence in the solar wind with SWOOPS will contribute not only to a detailed understanding of the heliosphere, but to an understanding of other astrophysical objects as well.

The Ulysses survey of the variation of interplanetary microstructure with heliographic distance in the ecliptic is well underway; the survey will soon be extended to higher solar latitudes after Ulysses encounters Jupiter in February 1992. The results of the survey will provide constraints on theories of the origin, propagation, and dissipation of interplanetary waves and on theories of their role in large scale solar wind dynamics.

1.5. Internal state of the solar wind plasma.

One of the prime objectives of SWOOPS is to establish a global picture of the internal plasma state of the solar wind. The internal state is reflected as complex shapes of the ion and electron velocity distributions. Ion distributions range from isotropic Maxwellian to multiple streaming distributions. Electron distributions appear to be bi-Maxwellian with enhanced heat flux extensions along the magnetic field at higher energies. The distributions can often be modelled in terms of two relatively convecting components carrying significant amounts of free energy. This energy can be released by triggering of a variety of micro- instabilities, leading to wave growth which can react back on the particle populations. Such kinetic processes regulate the efficiency with which the plasma conducts heat and transports linear and angular momentum.

Observations of the internal state of the plasma are relevant to several physical and astrophysical disciplines. They place constraints on theories of the coronal expansion. SWOOPS measurement of the strongly beamed high energy electron component is used as an indicator of the large scale magnetic topology and may provide a measure of the interplanetary electrostatic potential at high latitudes. Whether the beam of high energy protons that is usually present at high speeds persists at high latitudes is of interest since this beam may cause local proton heating. Studies of such phenomena can contribute towards understanding how plasma turbulence develops and its nature in an astrophysical setting.

1.6. Heavy ion composition of the solar wind.

Under favorable low temperature conditions, determinations of the solar wind ion composition can be made from E/q measurements alone. Most of the time , the extensively studied heavy ion, He^{++} (also referred to in this paper as He ions, helium, and helium ions) can be resolved from the more abundant hydrogen ions, H^{+}, with great accuracy. Helium has a widely variable abundance, ranging from $<0.1\%$ to $>25\%$. The lower values are found in low-speed solar wind associated with the coronal streamer belt and magnetic field reversals, while the higher values are associated with transient coronal events such as flare-induced CMEs. Corotating high speed stream flows contain a nearly constant mid- range He abundance near 4.8%. Routine measurements to high heliographic latitudes on Ulysses will help to complete the picture of the global systematics of helium variability.

Although a secondary objective, SWOOPS measurements of heavy ion species, e.g. Fe^{+10}, at higher solar latitudes can contribute to several important problems of solar physics. A problem of particular interest concerns coronal hole electron temperatures at which the high speed stream ionization states are established. A determination of the Fe ionization state in high speed streams provides a measure of this temperature. Such a determination can be made by fitting the Fe ion distribution envelope, even when the individual Fe species are not completely resolved.

1.7. Solar-wind interaction at Jupiter.

The SWOOPS experiment was not specifically designed to study the solar wind interaction with Jupiter's magnetic field and the nature of the Jovian magnetosphere during the Ulysses encounter with that planet, because first priority had to be given to measuring the high latitude solar wind ions and electrons that will be explored after the encounter. However, substantial fractions of the magnetospheric electrons and ions in the Jovian system will fall within the energy and angular acceptances of the SWOOPS analyzers, so valuable observations will be obtained there, particularly in view of the fact that Ulysses will traverse a different path than those taken by the predecessor Pioneer and Voyager spacecraft. Benchmark measurements of the bow shock and magnetopause locations will be made for comparison with earlier flyby observations and with the measurements that are to be made later by Galileo. The Ulysses measurements throughout the Jovian system should contribute to a more complete understanding of the nature of the interaction at the var-

ious interfaces as well as the nature of the plasma flow within and along the outer flank of the magnetosphere.

2. The approach adopted for SWOOPS.

2.1. General.

To satisfy many of the objectives outlined in the previous section, it was clearly desirable to measure ion and electron 3D velocity distributions in very fine detail and with high time resolution. However, ever finer spectral detail is costly in terms of experiment temporal resolution, weight, power, complexity, and bit rate. Similarly, ever higher time resolution can be obtained only at the expense of spectral detail, complexity, and bit rate. The approach to the SWOOPS design was to attempt to strike a balance between the conflicting requirements so as to optimize the overall plasma science yield from the mission and support other Ulysses investigations while staying within available mission resources. In the following subsections, the natures of the plasmas to be encountered, which placed constraints on our design criteria, are examined. These distributions are, of course, from in-ecliptic measurements, but high speed solar wind is emphasized since it is expected that at high latitudes the flows will be somewhat similar to high speed flows observed in the ecliptic plane.

2.2. Hydrogen and helium ions, H^+ and He^{++}.

Within typical low and high speed solar wind flows, the He^{++} ions, which usually have local temperatures four to six times higher than those of the H^+ ions, can be resolved in E/q spectra into separate hydrogen and helium components, except in unusual cases like one discussed below. They are less resolved in interaction regions at the leading edges of high speed flows, but it is expected that at the high latitudes to be reached by Ulysses the interactions between high and low speed streams will be both less intense and less frequent.

A survey of solar wind spectra shows that it is not unusual to find H^+ velocity distributions that cannot be described adequately by models consisting of simple extensions to a bi-maxwellian shape which includes a third velocity moment. Instead, the distributions can frequently be best described in terms of two separate solar wind streams flowing together with somewhat different speeds. For such cases, the spectra reveal two components, usually incompletely resolved, which drift relative to one another at approximately the local Alfvén speed. Striking examples of double stream flows that are relatively well resolved are illustrated in Figure 1, which shows two E/q spectra obtained about four hours apart with the Los Alamos solar wind plasma experiment carried on IMP 6. In the spectrum on the left, the H^+ ions in the higher speed flow have a density of less than 10% that of the slower component. In this unusual example, the hydrogen and the helium ions of both of the flows are resolved. Most often, as in the spectrum on the right, obtained after the flow speed had decreased by 30–40 km/sec, even though a helium group can be resolved from the two H^+ groups, the two He^{++} components are unresolved. Instead, they appear, as in the right spectrum, as a single component convecting relative to, and generally faster than, the H^+ ions.

It is interesting to note by inspection of Figure 1, that in four hours a large change occurred in the density ratios of the faster and slower streams. The amplitude of the faster H^+ stream in the left spectrum increased from less than 10% of the slower one to over 100% in the later spectrum on the right. Also note that the helium abundance, i.e. the He^{++}/H^+ ratio, in the two resolved streams in the left hand spectrum is apparently much higher in the faster, less dense stream. This is of particular interest, since it is evidence that bears on the sources of the two streams.

2.3. Heavy ions.

Measurements of heavy ion spectra with the solar wind plasma experiment on Ulysses at those times when kinetic temperatures are low enough that individual ion species can be resolved in E/q spectra will add to the body of knowledge already assembled from various experiments. These experiments include the Los Alamos Vela 3 through 6 electrostatic analyzer instruments, which were the first to resolve the minor ions, $3He^{++}$ and $4He^{+}$, and the heavy ions of oxygen, silicon and iron, extending in M/q from O+7 to Fe^{+7}. It is expected that the SWOOPS measurements will supplement those of the Ulysses SWICS composition experiment which does not have to depend on low local temperatures of the ions, as does SWOOPS.

Of particular interest for Ulysses, as noted previously, is the determination of the coronal temperature range over which the Fe ionization state is established as the high speed solar wind expands from coronal holes at high latitudes. Simulated heavy ion spectra, two examples of which are shown in Figure 2, demonstrate the feasibility of determining coronal hole 'freezing-in' temperatures from E/q spectral measurements of the Fe ionization state, even under adverse conditions. These simulations do not include the H^+ ion peak but do include ions of 14 other elements ranging from He to Ni. The assumed He^{++} local temperatures for the calculations are shown beside those peaks; local temperatures of the heavier ions were assumed to be proportional to mass on the left and independent of mass on the right. From top to bottom in each panel, the ionization states are assumed to have been established at coronal electron temperatures of 1.5, 2.0, and 3.0 $\times 10^6$ K. Inspection of the simulations shows that

even if in the high speed streams the heavy ion local temperatures should be proportional to mass, it should still be possible to determine the envelope of the iron ion species sufficiently well to establish an ionization state temperature, or range of temperatures. If the ion species should be individually resolvable, as in the right panel of the figure, the determination will be even easier. To resolve the individual peaks well requires an experiment resolution, $\Delta E/E$, of about 2.5%.

2.4. Solar wind electrons.

Solar wind electron velocity distributions measured in the ecliptic are complex, usually exhibiting a central, low energy 'core' distribution embedded in a higher energy 'halo' distribution. Most often, a beamed, unidirectional heat flux component is also present in the distributions, carrying energy from the hot corona out into the colder interplanetary space along the interplanetary magnetic field. Sometimes, the heat flux is observed to be counterstreaming, or bidirectional, due to unusual coronal/solar wind conditions, such as the presence of CMEs propagating past the spacecraft (S/C). At other times, the heat flux electrons disappear from the distributions, suggesting field merging and disconnection sunward of the S/C. These heat flux features contribute important information on the global magnetic topology of the IMF, on the nature of the interplanetary solar wind, and on its source.

Since virtually no information is available concerning the nature of electron distributions at higher latitudes, ecliptic results are taken as the baseline for Ulysses. The left panel of Figure 3, shows cuts along the magnetic field direction of a typical distribution fitted with bimaxwellian distributions, using three assumed S/C potentials, identified in the figure. A S/C potential of 4.5 V gives the best fit at this time. The functional fit shows the commonly observed low energy or 'core' component and higher energy but lower density 'halo' component. It should be mentioned that other functional forms are sometimes used to fit the halo, but a discussion of them is beyond the scope of this instrument paper.

As mentioned, a high energy 'heat flux' or 'strahl' component, strongly beamed along the interplanetary magnetic-field direction, is often observed. An example, measured with IMP 7, is shown in the right panel of Figure 3, in which angular cuts at different energies are given. For these spectra the measurement points were separated by 11.25°. In the design of the Ulysses experiment, as discussed later, care was taken that there would be no coverage gaps large enough for beams like this to be missed. Referring to the figure, the decreasing angular width with increasing electron energy exhibited by the beam in this example appears to be well described in terms of a collisionless expansion of the high energy electrons in which both the magnetic moment and total energy are conserved.

3. Instrumentation – general.

Electron and ion measurements are made simultaneously with two completely separate instruments. This provides an important measure of redundancy since solar wind bulk flow parameters can be derived from measurements made with either instrument. Each is separately powered, with its own low-voltage converter, multiple fixed-level analyzer voltage supply, and CEM high voltage (HV) supply. Each is operated with an independent microprocessor-based electronics control and data handling system.

Each instrument makes use of a curved-plate electrostatic analyzer with a spherical section geometry that is cut off in the form of a sector. For a sector, particle bending angles from the center of the entrance aperture to the exit of the plates are the same, independent of the entry angles. Each analyzer is equipped with a number of CEMs arranged around the analyzer exit to intercept analyzed particles which have entered the analyzer within a fan-shaped solid angle of acceptance. The instruments are oriented on the S/C so that the planes of symmetry of their acceptance fans are parallel to the spin axis. Particle arrival directions, then, are measured in a S/C coordinate system of azimuth angle, scanned by S/C rotation, and polar angle, determined by which CEMs intercept the particles. Azimuth angle is measured from the spin angle at which the Sun is included in the center plane of the acceptance fan and polar angle is measured from the spin axis, which constantly points toward the Earth. The local polar and azimuth angles will, of course, be converted to appropriate frames of reference for analysis.

Spacecraft and mission design parameters were important drivers of the specific designs of the two instruments. The most critical driver was the necessity for maintaining the S/C spin axis pointed at the Earth throughout the mission. As discussed later, this feature greatly complicates the design of the ion analyzer experiment. Another important mission feature is the spin period of the S/C, nominally 12 s, which determines the basic timing patterns of experiment cycles. Of critical importance, the S/C data rates, 1024 bits/s during tracking and 512 bits/s during store periods, constrain the bit rates that could be allotted to the plasma experiment, limiting the time and spatial resolutions that can be achieved. Of the 1024/512 bits/s totals, the plasma experiment is allotted 160/80 bits/s, divided 112/56 bits/s for ions and 48/24bits/s for electrons. Time resolutions achieved are discussed in the individual instrument descriptions.

The wide range of heliocentric distances covered during the mission, 1 to 5 AU, was another important driver because each experiment had to be designed to provide a dynamic range that covers not only the normal hour-to-

hour and day-to-day particle flux intensity variations, but in addition covers the factor of 25 variation in $1/R^2$ that will occur over the lifetime of the mission. As discussed later, different solutions for this problem are used for the two instruments.

4. Ion analyzer experiment.

4.1. General characteristics and physical description.

Solar wind ion measurements are made with a spherical section electrostatic analyzer shown schematically in Figure 4. Ions that pass through the entrance aperture with proper angles are selected in E/q by applying appropriate voltages across the curved plates. They are selected in polar angle by the CEMs in which they are detected, and in azimuth angle by the spin angle at which they are detected, referenced to the solar direction.

The analyzer, cut off to provide bending angles of 105° from the center of the entrance aperture for all entrance angles, has an average radius of 100 mm and a plate spacing of 2.84 mm. An angle of 105° was selected to give good resolution and slightly overlapping responses from the 16 CEMs arrayed behind the analyzer with 5° spacings. To avoid backgrounds caused by UV reflections through the plates to the CEMs, the plates are copper plated and blackened. The analyzer is mounted on the S/C so that the first CEM views along the spin axis direction and the sixteenth at 75° from the pole. As discussed later, appropriate sets of the CEMs are selected for data collection and transmission as the mission progresses and the angle between the spin axis and the Sun changes. The intrinsic FWHM energy resolution is about 5%. Because of various factors, which include the 1–5 AU variation in heliocentric range during the mission, the spin period of the S/C, the maximum allowable CEM counting rates, etc., the necessary dynamic range of the experiment cannot be accommodated simply by varying the length of the multiplier counting intervals. Hence, a set of seven apertures is provided on a disk driven by a stepper motor that can be commanded to select appropriate aperture sizes as the mission progresses. The wheel includes a blank position that was used during launch and can be used for inflight background measurements.

The CEMs are powered by a −2400 V to −4000 V HV supply with 16 commandable voltage levels for inflight CEM gain adjustment, as necessary. Negative high voltage is used to post accelerate the ions into the CEMs so that they are counted with high efficiency. The CEMs are operated at average gains of 5–10 × 10^7 electrons per pulse, and the pulses are amplified with discrete component amplifier-discriminators with threshold sensitivities of 10^{-13} coulomb. Experiment control and data handling are implemented with an 1802 microprocessor-based logic with read-only (ROM) and random-access (RAM) memories. Counts, collected in 16-bit serial registers from the 16 CEMS, are coded into 8-bit words for those channels that are selected as described in the next section and stored in memory for readout to the S/C data handling and telemetry system.

Analyzer high voltage is provided by a 200-level supply with levels extending from −15.3 V to −2070 V to cover a range of central energies extending from 255 eV/q to 34.4 keV/q. Level spacings are 2.5%, and the levels are used in several different ways, as discussed later. In some data cycles, the analyzer supply operates in an active range-adjusting mode which makes more efficient use of the experiment bit rate. The voltage level at which the solar wind H^+ peak produces the highest counting rate is determined in each measurement cycle and used to set the E/q range to cover H^+ and He^{++} ions in the next cycle. The H^+ peak position also determines the measurement ranges for two other cycles used for measuring heavy ions.

As mentioned previously, a motor-driven disk with seven different apertures is used to adjust the experiment dynamic range as heliocentric distance changes. The appropriate aperture for standard operation at a given heliocentric distance is selected by command. In a special high-sensitivity mode for heavy ions, discussed in Section 4.5, the largest aperture is selected.

For flexibility during experiment preparation, the experiment design is modular. Figure 5 shows a photograph of the 4.1 kg instrument which is composed of a drum–shaped sensor box which is tied to a rectangular electronics box by means of triangular brackets. The sensor contains the electrostatic analyzer, CEMs with amplifier-discriminator circuits, stepper motor, and aperture wheel. The electronics box contains a low voltage converter, a 200-level analyzer plate voltage supply, a 16-level CEM HV supply, microprocessor-based electronic control and data processing systems, and auxiliary timing and interface circuitry. Interconnections between the packages are made via cable connectors and tie points in such a way that the units could be easily joined or separated during ground testing, with no soldering or major disassembly required.

4.2. Solar wind-spacecraft reference frame.

Because of the Ulysses requirement for keeping the body-fixed high gain antenna pointed towards the Earth, a particularly difficult geometry for a solar wind ion experiment had to be accommodated. In the past, solar wind ion measurements have most often been made on a spinning S/C with its spin axis inertially fixed, generally perpendicular to the ecliptic. For such a S/C, 3D measurements of the ion velocity distributions can be made with an electrostatic analyzer equipped with eight or nine CEMs with 5° spacings. The analyzer is oriented so that with

each spin its fan-shaped acceptance angle is carried past the Sun with the solar direction centered in the multiplier array. For such a geometry, the experiment generates an invariant three-dimensional rectangular array, or 'matrix', of counts as a function of spin or azimuth angle, CEM number or polar angle, and analyzer voltage level or E/q. Fitting this data matrix allows a determination of the various ion parameters sought, such as bulk velocity, number density, parallel and perpendicular temperatures, etc.

Contrasting with an inertially oriented S/C is the Earth-oriented Ulysses geometry. Throughout the mission the angle between the solar direction, which is approximately the average direction of arrival of the solar wind, and the Earth-pointing S/C spin axis, changes continuously; this Sun Aspect Angle (SAA) ranged from above 75° shortly after launch, to values which oscillate near 0° as the S/C nears Jupiter. As the S/C passes over the solar poles, the SAA will range up to 25° during the south polar passage, and up to 30° for the north passage.

Figure 6 gives a polar representation of the geometry and highlights the difficulties for a solar wind ion experiment on Ulysses. The solution to making adequate measurements is based on the fact that roughly 5° spatial resolution is required in both polar angle and azimuth to make adequate solar wind ion measurements. At times, even higher resolution would be desirable, but compromises had to be made between various factors including experiment complexity, time resolution, and bit rate usage. In this representation the pole represents the spin axis at 0°; this axis points toward the Earth constantly. Concentric circles at 5° intervals represent the arcs swept out during each revolution of the S/C by the 16 CEMs located as shown in Figure 4 and depicted in Figure 6 by the larger dots aligned vertically upwards from the spin axis.

The basic operating cycle makes use of the S/C Sun sensor and spin clock to divide each revolution into 64 parts or sectors depicted in Figure 6 by the lines radiating from the spin axis. As shown in the next section, a basic measuring pattern is implemented by using the S/C Sun clock sector pulses and the experiment time clock. During a spin, the numbers of counts accumulated in 35-ms intervals from each of the 16 CEMs are recorded at each energy level of a 4-level sequence that is initiated at every sector. Thus, every intersection of a circle with a radial line in the figure shows where a 4-level measurement sequence is initiated. There are a total of 1024 intersections or measurement points every S/C revolution. Since the accumulated counts at many of these points are zero, because they are taken with SWOOPS facing away from the solar wind beam, the efficiency of use of the bit rate allotment could be improved. The sectors are timed from the Sun pulse so that the Sun always falls at sector 32.5 and a subset of relevant data points within a range of ±20° of that central meridian, marked with the smaller dots, was selected from which data can be chosen for storage and transmission to Earth. A range of ±20° was chosen because the solar wind direction almost always falls inside that range. This selection reduced the number of data points that have to be covered from 1024 to 185 for SAAs falling between 0° and 60°.

Still, if the most efficient use is to be made of the allotted data rate, i.e. if the highest experiment time resolution is to be achieved within the bit rate allotment, it is desirable to limit further the number of data samples to be transmitted. This is achieved by dividing the 185 intersection points into 11 sets, or 'matrices', of 79 points each, centered on CEM positions from 2 to 12. Figure 7 shows four of the eleven matrices (MX_n), MX_0, MX_3, MX_6, and MX_{10}. MX_0 is designed for those times when the solar direction, SAA, lies between 0° and 7.5° of the spin axis, MX_3 for SAAs between 17.5° and 22.5°, MX_6 for 32.5° to 37.5°, and MX_{10} for SAAs starting at 52.5° and extending outward. These matrix arrays are implemented in logic data processing by selecting data output from appropriate CEMs and sector angles for storage and transmission. The matrices are stored in read-only memories (ROMs) in the electronics logic system, and are available for call-up by command as the mission progresses and SAA changes.

It is interesting to note in Figure 7 that the form of the data matrix changes from a nearly polar coordinate format for MX_0 to almost a rectangular coordinate format for MX_{10}. A different data analysis program is required for each of these 11 matrices, greatly complicating data reduction and placing severe limitations on the sophistication of analysis algorithms that could be implemented for the Common Data File. Finally, it should again be noted that, as described in the next subsection, each of the data points discussed above actually represents four different measurements at four different energy levels (and four slightly different angles). Thus, each data matrix contains $4 \times 79 = 316$ data points, and a complete set of measurements acquired in 10 spins contains 3160 data points.

4.3. Standard solar wind (SW) sequence search (S) and track (T) cycles.

The SWOOPS normal SW sequence of operation includes three types of operating cycle; two of these cover the H^+ - He^{++} E/q range, and another covers the heavier ions of oxygen, silicon, and iron. These cycles, to be described in detail below, are (1) the Search or S-cycle, which periodically updates the H^+ peak position and at the same time provides data from a wider range of E/q, (2) the Track or T-cycle, which brackets the H^+ and He^{++} peaks with an E/q range that is continuously adjusted up or down for solar wind speed variations, and (3) a Heavy Ion or HI-cycle, which is discussed in the next section.

Another more sensitive cycle for heavy ions, the H-cycle, discussed in Section 4.5, is run infrequently on command. Exact details of these cycles depend on whether the S/C is actively transmitting or in the data storage mode.

When the S/C is being tracked, the SW sequence consists of a leading S-cycle to determine the proton peak position, followed by eight track cycles, during which the E/q range is continually updated. When the S/C is in the store mode, the sequence order is changed to an S-cycle followed by four T-cycles. As described later, subcycles of the HI-cycle are interspersed with the T-cycles, so that at the end of a sequence, one complete HI-cycle has been obtained.

Both the S- and the T-cycles acquire identical 3160-byte sets of data in 10 spins of the S/C, independently of whether the S/C is being tracked or is in the store mode. However, the data acquired in 10 spins requires 20 spins, or 4 min, to transmit when the S/C is being tracked, and 40 spins, or 8 min, to transfer to the tape recorder when the S/C is in the store mode. With little penalty in overall time, this additional time is utilized to acquire low bit rate HI-cycle data, either when the S/C is being tracked or is in store mode.

An almost identical pattern of stepping through 40 levels of the 200-level analyzer voltage supply, four levels at a time each spin, is used for the S- and T-cycles. The major difference between S- and T-cycles is the level spacings. Figure 8 shows the voltage stepping pattern for a T-cycle. In the defined E/q range, every second level is used, so E/q spacings are 5%. At every sector edge during a spin, a 4-level sequence of analyzer voltage stepping is repeated while counts are accumulated at every level into 16-bit registers from all 16 CEMs in 35-ms counting intervals. Depending on the selected matrix of coverage, discussed in the previous section, counts from appropriate CEM registers at selected sectors are compressed to 8-bit words in the microprocessor-based logic, stored in experiment memory, and later shifted to the S/C for transmission or to the tape recorder. In the first spin of a T-cycle, counts are accumulated beginning at the lowest level of the pattern; this level is continuously adjusted up and down for solar wind speed variations by tracking the proton peak. The level number, $L_{\max}$, at which the maximum count (proton peak) is recorded is determined in each T-cycle and used to establish the first level of the succeeding cycle in such a way that the cycles alternate using the odd, O, and even, E, levels of the supply. When conditions are stable, the complementary sets of data can be interleaved to give level spacings of 2.5%, the highest resolution available.

The T-cycle E/q range brackets the solar wind ions as illustrated in the Figure 8, which shows two spectra of counts vs. E/q plotted vertically at the side of the figure. One of these spectra is typical of times when local temperatures are low and the two major solar wind species are very well resolved; the other is typical of times when the H^+ and He^{++} ion peaks are warm and not so well resolved. The E/q range of the T-cycle is designed to accommodate such variations as well as those cases when the He^{++} ions are travelling faster than the protons by approximately the Alfvén speed.

The S-cycle pattern is the same as the T-pattern, except that it uses every fourth level of the analyzer supply, instead of every second level as in the T-cycle. The S-cycle levels are a fixed (F) set which always begins at the lowest level, level 1, of the supply on the first spin, and ends at level 157 on the 10th spin. With 10% level spacing, the 40 levels of the S-cycle cover central E/q values from 255 eV/q to 11.9 keV/q, or taking the FWHM response widths of the analyzer into account, the full range is 248 eV/q to 12.2 keV/q. Again, at every sector edge during a spin, a 4-level sequence of analyzer voltage stepping is repeated, while counts are accumulated in 35-ms counting intervals at each level. As mentioned, when the S/C is transmitting, the basic SW sequence begins with a 20-spin Search or S-cycle, which is actually composed of two subcycles. In the first 10 spins, a 40-level cycle using every fourth step is covered and the proton peak position, $L_{\max}$, is determined with 10% resolution. This 10-spin subcycle is followed by a second one, which, like the T-cycle, uses every second level to obtain a refined $L_{\max*}$ to 5% accuracy. This $L_{\max*}$ is used to determine the levels for the first T-cycle of the sequence and retained for use in all of the HI subcycles throughout the sequence. The wider range S-cycle data from the first subcycle are transmitted, but those from the second subcycle are not because of data rate limitations.

4.4. Heavy ion HI-cycle.

Routine HI-subcycles for heavy ions are run during the extra 10-spin (transmitting) and 30-spin (store) periods that must follow T-cycles to allow time for data to be shifted out for transmission or tape recording. Data from each HI-subcycle are combined with and telemetered with the T-cycle data that precede the HI-subcycle. The full HI-cycle is formed by combining eight HI subcycles, all of which are based on the E/q level of the proton peak, $L_{\max*}$ that was determined in the second S subcycle at the beginning of the sequence. That $L_{\max*}$ position establishes a set of 64 levels separated by 2.5%, designed to cover heavy ions ranging from O7+ with $M/q = 2.29$ to Fe^{6+} with $M/q = 9.3$. Each individual subcycle covers eight energy levels. To illustrate the sequence, the subcycles are designated '1' for levels 1–8, '2' for levels 9–16, '3' for levels 17–24, etc. A subcycle consists of eight spins during which the designated analyzer voltage levels step up once per spin. Counts from the individual CEMs are integrated during each spin over the designated sector range and stored for shifting to the S/C according to the

commanded data matrix. Each subcycle generates up to 72 bytes of data. At the end of a sequence of eight HI subcycles, the entire 64-level HI-cycle heavy ion spectrum, integrated over spin angle, has been accumulated.

During S/C tracking periods, one HI-subcycle is run with each T- cycle, with subcycles identified with a number between 1 and 8. As previously noted, there are two types of T-cycle, identified as E or O that use even and odd levels alternately. The SW sequence of cycles, then, including an initial search cycle, can be written as

S/C-transmitting SW Sequence: S - O_1- E_2 - O_3 - E_4 - O_5 - E_6 - O_7 - E_8.

This sequence produces an S-cycle matrix of data, eight T-cycle matrices, and a 64-level HI spectrum of data. While the S/C is transmitting, the sequence repeats over and over, with occasional interruptions when the higher sensitivity heavy ion H-cycle, to be described in the next section, is commanded to run one cycle. The nominal time for a complete S/C-transmitting SW sequence is 36 min.

During S/C data store periods when the data rate is reduced to half, instead of 10 additional spins being required to shift out data from each cycle, 30 additional spins are required. This extra time is used to fit in two HI-subcycles with each E and O T-cycle. The SW sequence of cycles for store periods is then

S/C-store SW Sequence: S - O_{12} - E_{34} - O_{56} - E_{78}.

This 40-min S/C-store mode SW sequence, like the S/C-transmitting SW sequence, contains an S-cycle and a 64-level HI-cycle spectrum, but unlike the S/C-transmitting sequence, it contains only four T-cycles instead of eight.

4.5. Heavy ion H-cycle.

The heavy ion, H-cycle, which operates on command, places SWOOPS in its most sensitive configuration by stepping the aperture wheel to its largest opening. An E/q range of levels that avoids the proton peak position is used to avoid running the multipliers at excessive counting rates. This range is established using the latest proton peak position, L_{max}, determined in the last T-cycle before the H-cycle begins. The cycle is similar to the HI-cycle, except that after stepping to the largest entrance aperture, the 64 E/q levels that cover the expected positions of O^{7+} to Fe^{6+} are run in eight groups of eight-spin subcycles in succession without interruption, one level each spin. Instead of integrating counts over the entire spin range designated by the commanded data matrix, as in the HI-cycle, in the H-cycle counts are integrated between the defined sector edges. Thus, the H-cycle provides the best heavy ion data, since it is run not only in the most sensitive experiment configuration, but it also provides angular resolution in azimuth. The duration of the cycle is 12.8 min. The number of data bytes produced in a 64-spin H-cycle is 64 levels × 79 matrix points, or 5056, in eight separate groups, each preceded with sync identification. Because the cycle takes a relatively long time, and because it is desirable to limit the frequency of stepper motor operation, the H-cycle is commanded to run only once or twice per day.

4.6. Ion measurement accumulation and repetition times.

The four measurement cycles for ions that produce data matrices for scientific data analysis are: (1) the Search, S-cycle, (2) the Track, T-cycle, which uses alternating even, E, and odd, O, analyzer levels, (3) the Heavy Ion, HI-cycle, formed from HI-subcycles 1-8 obtained during an SW sequence, and (4) the Heavy ion, H-cycle, which uses the largest aperture.

As described previously, these cycles are combined together into sequences that differ somewhat for times of S/C tracking and those of data storage. The cycle accumulation and repetition times for S/C tracking and storage times, along with other characteristics, are given in Table 1.

4.7. Ion analyzer response and calibration.

The angular and E/q response functions for the individual CEM positions were obtained with pre-flight laboratory calibrations in the Los Alamos plasma analyzer calibration facility. The analyzer was mounted on an externally controlled two-axis table within a calibration chamber with the instrument entrance aperture centered in a beam from a 1–30 keV duoplasmatron ion source with a monitored flux intensity and fixed energy. The calibration was performed by setting the instrument at various orientations with respect to the particle beam and collecting files of the fraction of the beam transmitted as a function of plate voltage. By covering angle space with suitable resolution, a three-dimensional matrix of transmission in polar angle, azimuth, and E/q space was built up for each of the 16 CEM locations. This collection of 16 matrices, combined together, constitutes a matrix that fully defines the instrument's response function. Because the number of individual measurements necessary for such a comprehensive calibration of an instrument having 16 independent sensors and various sizes of entrance apertures is so large, it was not possible to do the calibrations manually. Instead, they were done with a specially developed, computer-augmented system that automatically programmed the measurements, gathered and displayed the data, and recorded it for further analysis in a large computer. The total number of information bits contained in the ion instrument calibration is nearly 10^8. These calibrations are used to convert the matrices of data obtained in flight into meaningful parameters such as density, flow speed and direction, and components of the temperature.

The calibrated polar angle responses of the 16 CEMs are shown in Figure 9. The responses were obtained by setting the analyzer for maximum response with energy and azimuth angle and then sweeping through polar angle, keeping the particle energy and azimuth constant. This corresponds to one column taken through the full response matrix parallel to the polar angle axis.

The FWHM values of the polar angle responses of the various CEMs are ~4.7°. The average center-to-center spacing of the CEMs is 5.2°, in good agreement with the 5° design spacing. Cuts taken through the full response matrix parallel to the azimuth angle axis show the azimuth FWHM values of the various detectors ranging from 3.1° in the central locations to 4.5° at the polar angle extremes. Such a broadening of azimuth response with polar angle is expected on the basis of mathematical analysis. The broadening, taken together with the observed reduction of transmission with polar angle (Fig. 9), results in similar total integrated responses at each location.

In the final direction through the response matrix, parallel to the E/q axis, FWHM energy resolutions of ~4.8% are found, in good agreement with the expected values. The complete calibrated response, measured in great detail but not shown here, is used for analyzing flight data.

5. Electron analyzer experiment.

5.1. General characteristics and physical description.

Solar wind electron measurements are made with a spherical section electrostatic analyzer, shown schematically in Figure 10. Electrons that pass through the entrance aperture with proper angles are selected in energy with appropriate voltages applied across the curved plates. They are selected in polar angle by the seven CEMs in which they are detected, and in azimuth by the spin angle at which they are detected, referenced to the solar direction.

As shown in the right view, the FWHM acceptance angle of the analyzer in azimuth depends on polar angle; at 0° it is 9.1° and at 73° it is 28.7°. The analyzer is mounted in the S/C with its fan-shaped acceptance solid angle oriented so that the plane of symmetry of the fan is parallel to the spin axis and the CEM at the defined 0° position views perpendicular to the spin axis.

The 120° analyzer has an average radius of 41.9 mm and plate spacing of 3.5 mm. The intrinsic FWHM energy resolution is ~13%. Unlike the ion instrument, which requires a variable aperture size, it is possible to accommodate the dynamic-range requirements of the electron instrument, imposed by the 1–5 AU heliocentric range variation, by simply changing the duration of the counting interval by command. This easier solution, compared to that for the SWOOPS ion experiment, is due principally to the fact that electron distributions are comparatively broad, so the counts are spread over all of the CEMs, energy levels, and azimuth angles, instead of being concentrated in a tight beam in angle and energy, as is the case with the ions.

The seven CEMs are powered with a +2400 V to +4000 V HV supply with 16 commandable levels for inflight CEM gain adjustment. Positive high voltage is used in this case, with the CEM funnels biased at +200 V to provide post acceleration of the lowest energy electrons so as to count them with high efficiency. The CEMs are operated with gains of 5–10 $\times$ 10^7 electrons per pulse. Discrete component amplifiers and discriminators with threshold sensitivities of 10^{-13} C are used to amplify the pulses. Normalized pulses are counted in 16-bit serial registers, coded into 7-bit words, and stored in memory in an 8-bit format for readout to the S/C data handling, storage, and telemetry system.

The analyzer plate voltage, which is applied to the inner plate, is provided by a 30-level supply with levels extending from +0.19V to +180 V, giving a central energy range of 0.86 eV to 814 eV, or a total range of 0.81 eV to 862 eV, when account is taken of the response width of the analyzer. Standard electron measurement cycles use one of two sets of 20 energy levels that can be selected by command. The central energies of one set extend from 0.86 eV to 429 eV, and the other from 1.7 eV to 814 eV. In another commandable mode, the two sets of energy levels are used in an alternating sequence. Backgrounds caused by UV scattering through the plates and by photoelectron and secondary electron production in the analyzer plates themselves can contaminate the data to greater or lesser extents, depending on design. The analyzer plates for the electron instrument are grooved, in addition to being blackened, to keep the contamination level low. Grooving was not necessary for ions because of the tighter geometry. Additionally, a special mode of operation is provided to measure the background by applying a +9.7 V voltage source to the outer, normally grounded plate. In conjunction with this, there are special, closely spaced analyzer voltage levels for the inner plate, beginning just above the +9.7 V level applied to the outer plate. In a special 'photoelectron' (Ph) cycle that can be operated periodically, the outer plate voltage is turned on and the Ph levels of the analyzer supply exercised. In this configuration, all electrons entering the analyzer from outside are accelerated and thus have energies $\geq$9.7 eV, while background photoelectrons and secondary electrons produced within the analyzer itself with energies generally below 9.7 eV will be unaffected. Thus, the numbers and energy spectra of these background electrons generated within the plates are determined for subtraction from the data.

For flexibility, the experiment design is again modular, as shown in the Figure 11 photograph. The 2.6 kg package is mounted on the S/C equipment platform inside the S/C

body with the entrance aperture exposed through holes in the side panel and a local thermal control blanket. The drum-shaped sensor package which contains the analyzer plates, CEMs, and associated amplifier-discriminator circuits is mounted on a chassis that is an integral part of a box-shaped electronics package. The sensor package is easily mounted or removed from the electronics chassis. The electronics box contains microprocessor-based logic cards, low voltage converter, analyzer plate voltage supplies, CEM HV supply , timing circuits, and interface circuits. Interconnections between sensor and electronics packages are made through a cable connector and tie points designed so that during the development and testing stages the units could be easily joined or separated with neither soldering or major disassembly required.

5.2. Solar wind – space craft reference frame.

For measurements of the broad distributions of solar wind electrons, no special problems are introduced by the Earth-oriented configuration of the S/C, unlike the case for measurements of the narrow, anti-solar directed solar -wind ion beam. Referring again to Figure 10, the analyzer is mounted on the S/C with the CEM at 0° viewing along the S/C equatorial plane. The other CEMs view at central polar angles of ±21°, ±42° and ±63° with respect to the equatorial plane. A full polar angle range of over ±73° is covered without gaps, because, as will be shown later, the CEMs have overlapping responses. Because of the broad nature of electron velocity distributions, measurements must be made covering as much of the 4π sr unit sphere as possible, independent of the measuring reference frame. Therefore, in the case of the Earth-oriented Ulysses frame, all that is required after determining the electron velocity distribution in the spacecraft reference frame is to transform it into a universal solar-oriented reference frame.

5.3. Basic operating cycle of the electron spectrometer.

Two-dimensional as well as three-dimensional measurements are made to avoid the prohibitively long repetition times that transmission of 3D measurements alone would entail. Even so, repetition times are unfortunately long.

The basic operating cycle of the electron analyzer is illustrated in Figure 12. It is used to generate four different science data cycles. These cycles produce energy/angle matrices of counts with sufficient resolution that various desired parameters of the electron distribution, such as number density, temperature, distribution anisotropies, etc. can be accurately calculated. In the cycle shown in the figure, two analyzer voltage levels with 38% spacing are alternated 128 times during each spin. In the following spin, the next pair of levels is alternated. At the end of 10 spins, 20 electron energy levels have been sampled at two interleaved sets of 64 spin angles. Counts are taken from all seven CEMs every time that the voltage switches and are accumulated in 16–bit serial registers. Fixed counting times ranging from 4 to 64 ms, are selected by command. The S/C spin clock is used to divide the spin into 128 intervals, each spanning 2.8125° and a nominal time of 93.75 ms. Near 1 AU, 4-ms intervals were long enough to provide statistically accurate counts without danger of counter spills. As heliocentric distance increases and counting rates diminish, longer counting intervals are selected to maintain statistical accuracy.

The main reason for using alternating energy levels, as shown in Figure 12, rather than changing the level once each spin is to acquire the needed 20 levels of data in 10 spins rather than 20, so that the data accumulation and repetition times do not become excessively long. Because the electron beams, or 'strahl', that are found in high -speed solar wind can be quite narrow, the frequency of level alternation is kept high and counts sampling is done in such a way that a beam cannot be missed.

There is one exception to the alternating voltage pattern of operation. In a cycle designed to determine the gain conditions of the seven CEMs, the analyzer voltage is held constant while data are taken over 10 spins at a fixed electron energy. Five CEM HV levels centered on the presently commanded operating level, and two different amplifier threshold sensitivity levels, are utilized during the 10-spin cycle to determine the CEM gain conditions. If the cycle results indicate a need for higher gain, the CEM HV supply can be commanded to a higher voltage level. A similar gain calibration cycle is used to monitor the gains of the ion spectrometer CEMs.

5.4. Science data cycles.

There are four science data cycles called 2S, 3R, 3P, and 2P. The numbers 2 and 3 indicate the number of dimensions of the measurements; the letters have no special significance. The 2S- cycle gives the highest resolution in azimuth, which can be particularly useful for resolving very narrow beams. It is a two-dimensional cycle that operates as shown graphically in Figure 13, where the alternating level pattern for levels $L(n)$ and $L(n+1)$ is shown. Considering level $L(n)$ only, counts are accumulated from each CEM in the commanded counting interval every time that the voltage switches to $L(n)$. At the end of each counting interval, the counts from the seven CEMs are summed together, divided by 2, compressed to a 7-bit word, and stored in the experiment memory until shifted out to the S/C data-handling system. The same operations are done on the counts at $L(n+1)$, of course, and for all other levels during the 10-spin cycle. At the end of the cycle a data set of counts at 64 angles and 20 energy levels containing 1280 7-bit data words (1120 bytes), has been

accumulated. Ten bytes of sync and status information are included with each cycle of data. When the S/C is being tracked, the electron experiment bit rate is 6 bytes/s, so that a 2S cycle of data is shifted out in 3.14 min. In data storage periods at half the bit rate, the time is 6.28 min.

Although it would be very desirable to have a 3D cycle in which counts from all seven CEMs at 64 angles per spin are recorded and transmitted, the cycle readout time becomes prohibitively long. As a compromise, the 3R cycle (Fig. 13) generates data from each of the seven CEMs at 32 angles per spin. This is done by accumulating counts at level $L(n)$ in pairs of counting intervals, adding them together, compressing to 7-bits, and storing in experiment memory for readout. At the end of the 10-spin 3R-cycle, counts samples have been accumulated from seven CEMs at 32 spin angles and 20 energy levels to give a total of 4480 7-bit words (3920 bytes). To shift this data set, including status and sync words, to the S/C data-handling system takes 10.92 min when the S/C is being tracked and 21.83 min when it is recording data.

In the 2P- and 3P-cycles, counts at level $L(n)$ are accumulated in groups of four counting intervals as shown in the figure. For the 2P-cycle, the four-interval counts from each of the seven CEMs are summed and divided by 8 before compressing and storing. In the 3P-cycle, four-interval counts from each of the seven CEMs are compressed and stored. Thus, both cycles produce counts at 16 spin angles and 20 energy levels. For 2P, the total number of 7-bit words produced is 320, requiring 0.81 min or 1.61 min for readout. For 3P, 2240 7-bit words are generated, requiring 5.47 min or 10.94 min for readout. Various characteristics of these four science data cycles are summarized in Table 2.

Unlike the ion experiment which has just one standard operating mode, the electron experiment has two, selectable by command. One called RS, is designed to give higher spatial resolution; the other, called P, gives higher time resolution with less spatial resolution. The modes consist of three cycles in a sequence which repeats. They are listed in Table 3, along with pertinent times.

5.5. Electron analyzer response and calibrations.

The angle and energy response functions for each of the individual CEMs behind the analyzer must be known accurately to convert the data sets into useful electron parameters. The electron analyzer was calibrated in the Los Alamos plasma instrument calibration facility in an electron beam with fixed energy, in the same manner that the ion instrument was calibrated with ions. The polar-angle response results, shown in Figure 14, were obtained with a single sweep through polar angle with beam energy and azimuth angle set at values giving maximum response. Inspection of the figure shows that the geometry of the experiment provides overlapping response ranges, as desired to prevent measurement gaps in which a narrow electron beam, or 'strahl', might be lost or poorly resolved. With contiguous coverage in azimuth as the S/C spins, this polar angle coverage results in over 95% coverage of the 4π sr unit sphere.

Much more extensive response functions for each CEM location were, of course, determined from the laboratory calibrations and are used in analyzing the data. The FWHMs of the polar angle responses of the individual CEMs are ~19.5° and their calibrated locations are their design locations to within 2.5%. Cuts through the full response matrix parallel to the azimuth axis give FWHMs of the azimuth responses ranging from 9.1° in the center to 28.7° at the highest polar angles. Although the polar angle sweep shown in Figure 14 shows a large reduction in amplitude at the high polar angles, when the response broadening in azimuth is taken into account, the integrated responses of the CEMs from the center to the extreme locations are as expected. Cuts parallel to the energy axis show FWHMs for the energy responses of 11–12%.

6. Early flight results.

Following the launch of Ulysses aboard the shuttle Discovery on 6 October 1990, and its injection into an interplanetary orbit toward Jupiter by the upper rocket stages, mission and S/C constraints required a substantial waiting period before the SWOOPS electron and ion experiment packages could be activated. These constraints included S/C thermal considerations due to the early orientation of the S/C spin axis with the Sun, and the requirement for a long pumpout period to achieve clean, high vacuum conditions inside the SWOOPS sensor packages before operating the CEMs under high voltage. After some preliminary activities on 16 November, both packages were switched on successfully on 17 November, six weeks after launch. In this section, we present some early results to illustrate the types of data that are being received from Ulysses and to show the nature of the data products that are available from SWOOPS for carrying out the research aims of Ulysses during the three phases of the mission: the in-ecliptic cruise phase, the Jovian encounter, and the out-of-the-ecliptic cruise to high solar latitudes with passages over the south and north poles of the Sun.

6.1. Solar wind ions – E/q spectra and stacked plots.

As discussed in Sections 4.1 through 4.3, solar wind ion data from search or track cycles are obtained in blocks or 'matrices' of counts that cover selected polar angles (CEMs), azimuth angles (spin angle) and E/q (analyzer voltage) levels. Forty E/q levels with 5% spacings are

selected from the 200-level supply to span a range that is dynamically adjusted up and down to suitably bracket the ambient proton and helium ion peaks as their speed (energy/charge) varies. The most basic form of solar wind ion data is a matrix of counts covering 79 CEM-azimuth positions at each of the 40 E/q levels. A subset of such a matrix of counts, selected for an azimuth that gives a cut through the proton and helium ion peaks, is shown graphically in Figure 15. The spectrum shows counts collected from the CEMs at a single azimuth during 35-ms counting intervals as the analyzer voltage is stepped up, four levels per spin. Data from the individual CEMs are identified with different line types. The local temperatures of the protons and helium ions are low enough at this time that the peaks are cleanly resolved. Here, counts from the nine CEMs in the chosen matrix are plotted as a function of E/q step number, which is convertible into E/q values. To identify those step positions where the count is zero, points are plotted half a decade below the one-count level. The data set in Figure 15 was obtained soon after SWOOPS was turned on, when the matrix in use collected data from a set of nine contiguous CEMs.

Another form of solar wind ion data presentation that has been useful in the past and is being used to display Ulysses data, gives a pictorial representation of the flow conditions, as shown in Figure 16. This form, known as 'stacked plots', stacks E/q spectra vertically in a closely spaced time sequence, from top to bottom. Individual spectra are formed by integrating counts over CEMs and azimuth at each E/q level. Normally, the spectra show a prominent peak due to the protons with a second peak at twice the E/q that is due to doubly-ionized helium. Stacked plots present the data in a compressed form that makes such features as interplanetary shocks and other interfaces easy to recognize by sudden shifts in peak positions, broadening or thinning of spectral widths, changes in the relative sizes of peaks, etc. For example, in those rare cases when singly ionized helium ions, He^+, are present in substantial quantities, their presence is immediately obvious in a stacked plot by the unusual appearance of a third ion species peak at an E/q position four times that of the proton peak.

Figure 16 is a stacked plot from SWOOPS data for a 12-hour period from 1200 UT to 2400 UT on 23 November 1990. Inspection of the plot shows the expected proton and He^{++} peaks during a half- day when the speed is relatively constant, decreasing slightly from start to finish. The periodic, darker spectra are search-cycle data which cover a wider E/q range and reestablish the proton peak position every ninth cycle.This was a time of relatively high local ion temperatures, as shown by the somewhat broad proton and helium peaks that are only moderately well resolved. Although a good example showing an interplanetary shock or other pronounced feature is not yet available, the example given here shows a few features of interest and demonstrates the nature of the stacked plot presentation.

At the top of the figure, the first couple of spectra show a rapid, but small decrease in speed by the downward shift in the proton peak E/q position. At several other times there are some small, fast changes in speed and/or temperature which show up as extra white between spectra, e.g. at about 1530 UT, 1800 UT, and near 2100 UT. There are other times when the spectra show evidence that two solar wind streams were flowing together at this time, as discussed in Section 2.2 and shown in a much more striking example in Figure 1. Between 1800 UT and 1830 UT, the proton peak shows a 'dimple' which is evidence for a double stream. Near the end of the day, double stream shapes are again seen, and the very last spectrum clearly shows that the proton peak is made up of two overlapping distributions and there is a suggestion from the width of the helium peak that it also contains two groups.

6.2. Solar wind ions – velocity distribution moments.

Perhaps the most generally useful form in which solar wind plasma data can be presented is that of plots of velocity distribution moments, such as density, bulk speed, direction, temperature, etc. This form is often used for complementary studies which utilize data from other investigations and for in-depth studies of the underlying physics of space plasmas. Figure 17 presents ion moments for the second half of 18 November 1990, the first full day of operation of SWOOPS after it was turned on. The proton density, speed, temperature, and angles of flow are presented, along with the He^{++}/H^+ number density ratio , i.e. the helium abundance. Note that the polar and azimuth flow angles refer to a S/C coordinate system, where polar angle is determined by the CEMs from which measurements are taken, and azimuth angle is determined by the spin angles of the measurements, referenced to the plane in which the Sun lies. Features in this moment plot will be related to features in Figure 20 in the last section. Inspection of Figure 17 identifies a number of features of interest. For example, at 1400 UT, after a period of rising speed and fluctuating direction, there was a very sudden drop in speed that was not accompanied by significant changes in density or temperature. However, it was accompanied by the sudden appearance of a higher abundance of helium ions that was followed by a fluctuating abundance that reached a maximum shortly before 1500 UT. The moment data also show that these changes occurred during a time when there were strong fluctuations in the proton direction of flow. This feature is most likely a solar wind discontinuity, such as a tangential discontinuity, but further analysis is needed, perhaps including data from other investigations, before the nature of the discontinuity can be stated with confidence.

At about 1545 UT, there were rapid changes in speed coupled with strong changes of direction, but little change in density and temperature. Later, at about 1900 UT, there were sudden and substantial increases in density and temperature, coincident with a sudden swing in the azimuth direction of flow. Although changes like these are often associated with interplanetary shocks, in this case, that interpretation seems weak because the change in speed is so low. Again, further interpretation is needed to identify the type of this discontinuity.

There are, of course, other ways to display the ion data that are not illustrated here. For example, for some studies, contour plots of the velocity distributions can be very instructive. Such features as the alignment of parallel and perpendicular components of the temperature with the magnetic field, and heat flux tails on the distributions are shown well in the contour format.

6.3. Solar wind heavy ions.

As discussed in Sections 4.4 and 4.5, there are two cycle types included in the SWOOPS ion experiment for the purpose of gathering information on the heavy ions beyond He^{++}, including ions of O^{+7} and O^{+6}, Si^{+9} to Si^{+7}, and particularly Fe^{+12} to Fe^{+7}. Occasionally, in CME flows, ions of Fe^{+16} may be detected. These HI- and H-cycles make use of the measured proton peak position to establish the E/q range in which these ion species would be found. Generally, the HI-cycle provides rather low numbers of counts that will be mainly useful during times of long-term stable conditions when the local ion temperatures are low. A second heavy ion H-cycle, described in Section 4.5, is run on command using the largest aperture, and thus has the highest sensitivity.

A main objective for including these heavy ion measurements in the SWOOPS capabilities was to determine the coronal electron temperatures at which the iron ionization state is established, or 'frozen-in', as the high speed solar wind expands from the coronal holes. As is evident from the Figure 2 consideration of this problem, even if the local temperatures of heavy ions are too high for resolution of individual ion peaks, it should be possible to define the envelope shape of the iron ion species under favorable conditions and thus obtain an estimate of the coronal electron temperatures over which the ionization state was established.

Figure 18 shows the heavy ion spectrum that was obtained when the H-cycle was first run on 11 December 1990. Included in the figure are the positions of the proton and helium ion peaks, and the positions of various heavy ions that have been identified in earlier measurements of E/q spectra on Vela and other missions. At this time, local temperatures of the oxygen and silicon ions at the identified positions were too high for those species to be resolved. However, the group of iron ion species, lying beyond the lighter ions, is well separated from them and, indeed, some of the individual Fe ion peaks are close to being resolved. The envelope of the Fe lines yields an estimate, shown in the figure, of the span of coronal electron temperatures over which the iron ionization state was established, or 'frozen in'.

Analysis shows that the coronal electron temperature over which this Fe ion state was formed ranged from 1.0 to 1.5×10^6 K. Previous observations have established that this state tends to be broad, showing that the individual species pair ratios forming the envelope are established over a range of altitudes in a corona with a temperature gradient.

6.4. Solar wind electrons – energy spectra, velocity distributions, and moments.

As discussed in Sections 5.3 and 5.4, SWOOPS solar wind electron measurements are made with a cycle in which two energy levels are alternated 128 times in a S/C rotation; the level pairs step up each spin, so that in 10 spins, a full 20-level set of data is obtained. This set forms a basic matrix of counts at 64 azimuth positions (spin angle) and 7 polar angles (CEMs), for each of 20 energy levels (analyzer voltage). From these matrices, a number of two- and three-dimensional measurement cycles, named 2P, 2S, 3P, and 3R are formed, to make efficient use of the allotted telemetry rate. Although it would be desirable to send back all of the data from all seven CEMs with full angular resolution for each set of data, it is necessary to reduce the number of azimuth and polar angles for some of the sets as given in Table 2 to keep repetition times reasonably low.

Figure 19 presents a set of data from a 3P cycle of operation, selected at a fixed azimuth from a data set measured on 18 November 1990. Counts from the seven CEMs that were acquired at each of the voltage steps, are plotted. (The voltage step numbers are of course convertible to energy levels.) This plot shows the dominant features of solar wind electron data sets. Data taken from the seven multipliers as the energy is stepped up show a strong group of ambient, low energy photoelectrons surrounding the S/C with energies ranging from 0.86 eV to about 5.1 eV. Above the photoelectron distribution is the core distribution of solar wind electrons, discussed in Section 2.4, that emerges out of the low energy photoelectrons as they fall off. At higher energies, beyond the core, the less dense population of halo electrons is present. Two of the multipliers also observe a heat flux tail, identified by the elevated count rates at higher energies.

Not shown here are a few other forms for presenting solar wind electron data that can be quite useful for specialized studies. These forms include velocity distributions plotted as shown in Figure 3. For some studies, showing the velocity distributions in the form of contour

plots is a powerful way to bring out certain important features of the electrons, e.g. the heat flux and whether it is unidirectional, bidirectional, or missing. Contour plots can be particularly useful to illustrate how the electron distributions evolve with time during an event. Electron moments can be derived from the velocity distributions so as to display the time evolution of electron density, bulk flow speed and direction, parallel and perpendicular temperatures, heat flux , heat flux direction, etc., in a manner similar to the ion moments shown in Figure 17.

6.5. Solar wind electrons – color spectrograms.

Figure 20 presents a color spectrogram of electron data obtained in the period 1200 UT to 2400 UT on 18 November 1990. The vertical bars on the right of the spectrogram show the color codings for the counting rate levels of the top panel, above, and the rest of the panels, below. Universal time in hours is shown along the bottom with some pertinent ephemeris information. Included with the electron data is a spectrogram in the top panel labelled 'IONS', which shows ion E/q spectra extending over a total E/q range of 248 eV/q to 12.2 keV/q. This is the range of the search cycle when the intrinsic energy resolution of the analyzer is taken into account. Ion moments from the same time span are those given previously in Figure 17. Periodic light blue stripes extending from the bottom to the top in the panel, are spectra from the periodic search cycles. This 40-level cycle, which runs once every nine cycles in the solar wind sequence of operation, uses every fourth analyzer level starting at the bottom level of the 200-level supply. Thus, it covers a larger E/q range than the 40-level, dynamically adjusted track cycles which use every second level. These T-cycles form the narrower color band which contains the proton and helium ion distributions (see Sect. 4.3 for further details).

The second panel of Figure 20 shows a spectrogram of the energy spectra of solar wind electrons, extending from 0.81 eV to 862 eV. These data were obtained at a time when the two commandable energy ranges were being alternated, resulting in the dark 'box cars' along the bottom of the panel. Here, referring to Figure 19, the orange and red band at low energy is due to the ambient photoelectrons which produce the highest counting rates. Above the orange band, which first tapers off to yellow and then green as the photoelectron flux intensity falls off with increasing energy, lies a yellow band caused by the broad peak of the core distribution. Above the core distribution, the intensity of the halo flux falls off more slowly with increasing energy (see Fig. 19).

Panels 3, 4, 5, and 6 from the top, show angular distributions of the electrons in the four energy bands identified on the left. The bottom two panels give spectrograms of the counts distributions in the seven CEMs in two energy bands. Note that the resolution in those panels is broader, since there are only seven multipliers.

The features in this spectrogram can be inspected in combination with the ion moments in Figure 17. Starting before 1300 UT, the solar wind bulk flow speed began to rise, in concert with strong swings in the flow directions of the ions and angular variations in flux intensity maxima of the various energy bands of electrons, particularly the 212–454 eV band. Approaching 1400 UT, the speed increased from below 400 km/sec to 500km/sec and flattened off. At 1400 UT, the speed suddenly dropped to below 400 km/sec, coincident with a sudden increase in the helium abundance and a strong shift in the direction of 212–454 eV electrons. However, this change was not accompanied by changes in the proton density or temperature. This event is best interpreted as an interface in the solar wind, perhaps a tangential discontinuity, but not as an interplanetary shock. Further study will be required to determine the exact nature of this interface.

Later, shortly before 1600 UT, there were some fast fluctuations in the proton speed and direction at a time when the helium abundance had settled back down from high values to more conventional values. Again, the proton density and temperature do not change drastically, but the electron angular distributions show strong changes, mirroring the ion speed changes. Further study, which might include collaborative use of data from other Ulysses investigations, may help elucidate this behavior.

After this episode, the proton speed remained fairly constant for several hours while the density and temperature gradually fell, until just past 1900 UT, when both the density and temperature rose suddenly, along with a sharp change in flow direction. There were also strong shifts in the direction of the electron distribution maxima in the 5th and 6th panels of the spectrogram at this time. However, there was only a very modest increase in the flow speed. The spectrogram electrons at this time show an increase in the intensity of the color in all of the panels, which is an indicator of an increase in density and possibly temperature as well. Since the Figure 17 ion moment data show a density increase of a factor of two, as also exhibited in the top panel of the spectrogram by the appearance of the red band at about 1910 UT, the electron density must have increased also, which would account, at least in part, for the brighter yellow. Indeed, electron moment data that are not shown here show that the combined core/halo density did increase by a factor of two, but the electron temperature did not increase appreciably across the interface. Thus, it would seem that this solar wind discontinuity was not due to the passage of an interplanetary shock. Further study of these data, with the cooperative inclusion of data from other investigations, particularly the magnetic field investigation, is required before a firm interpretation of the nature of this discontinuity can be made with certainty.

6.6. COMPARISON OF ELECTRON AND ION RESULTS.

A good indication of the accuracy of the SWOOPS plasma measurements, made with separate instruments for electrons and ions, can be obtained by comparing the densities and bulk flow speeds determined independently with the two instruments. As shown in Figure 21, the electron and ion parameters compare remarkably well. Such agreement verifies the quality of the separate and independent calibrations of the two instruments and the integrity of the data analysis techniques. The small discrepancies are not surprising considering the various uncertainties inherent in measurements of this nature. One of the most important of these uncertainties is the distortion of the solar wind electron velocity distribution caused by a varying spacecraft charge. This effect can be quite significant for the Ulysses spacecraft which reaches potentials in excess of 5 V with respect to the ambient plasma medium in which the spacecraft is immersed. The level of charging is determined from the shapes of the photoelectron and core/halo electron distributions and used to correct for the distortion.

The top panel of Figure 21 shows electron and ion densities compared by plotting the occurrence distribution of N_e/N_i in bins of 0.02 for a 1250-spectrum data set obtained between 1.16 and 1.29 AU. The bottom panel shows the occurrence distribution of V_e/V_i. Ion number densities and speeds for comparison with electron number densities and flow speeds were obtained by combining proton and helium ion densities and speeds with appropriate weighting for charge. Electron measurements used in the analysis are for 3D data sets only; the analysis includes both core and halo distributions. Photoelectrons are of course removed in the analysis. Inspection of the figure shows that on average the electron and ion densities and flow speeds agree to within about 5%, which is surprisingly good agreement for independent experiments of this nature. The data show that significant deviations of 15% or more can occur; such deviations are probably due principally to inaccuracies in the determination of spacecraft potential.

Acknowledgements.

The Ulysses Solar Wind Plasma Experiment Coinvestigators and Associates include J. R. Asbridge (Los Alamos), S. J. Bame[1] (Los Alamos), A. Barnes (NASA/ARC), W. C. Feldman (Los Alamos), B. E. Goldstein[2] (JPL), J. T. Gosling (Los Alamos), T. E. Holzer (HAO), D. J. McComas (Los Alamos), M. Neugebauer (JPL), J. L. Phillips[3] (Los Alamos), H. Rosenbauer (MPAe), G. L. Siscoe (UCLA), S. T. Suess (NASA/MSFC), M. F. Thomsen (Los Alamos), and R. D. Zwickl (SEL/NOAA). We wish to acknowledge the help that has been provided to us by various members of this group, including participation in the definition of the original scientific objectives and preparation of the proposal. This team will participate together and with other Ulysses investigators on various scientific studies, as the Ulysses Mission continues.

We wish to thank the technical staffs at Los Alamos and Sandia for the support that has been provided in preparing the Ulysses Solar Wind Plasma Experiment. We also wish to acknowledge the guidance and support provided to us in a very professional manner by the Project Staffs at ESTEC, including K.-P. Wenzel, ESA Project Scientist, P. J. Caseley, Experiment Manager, and Derek Eaton, Project Manager, and at JPL, including E. J. Smith, NASA Project Scientist, T. Tomey, Experiment Manager, and Willis Meeks, Project Manager. This research has been done in part by the Los Alamos National Laboratory and the Sandia National Laboratories, Albuquerque, under the auspices of the US Department of Energy with financial support provided by NASA, and in part by the Jet Propulsion Laboratory, California Institute of Technology, under contract to NASA.

It is beyond the scope of this paper to give a comprehensive reference list of the many sources from which the investigation objectives, background, and other details in the paper were drawn. Such a list, if complete, would occupy more space than is available. However, it should be acknowledged that some of the material given in this paper is derived from an earlier description of the SWOOPS investigation given by S. J. Bame, J. P. Glore, D. J. McComas, K. R. Moore, J. C. Chavez, T. J. Ellis, G. R. Peterson, J. H. Temple, and F. J. Wymer: 1983, in The International Solar Polar Mission – Its Scientific Investigations, esa SP-1050, K.-P. Wenzel. R. G. Marsden, B. Battrick, ed., ESA Scientific and Technical Publications Branch, ESTEC, Noordwijk, The Netherlands, p. 47. Figures drawn or adapted from that source are acknowledged in the captions.

[1] Principal investigator
[2] Data analysis team leader, JPL
[3] Data analysis team leader, Los Alamos

TABLE I. *Characteristics of ion measurement cycles of the solar wind ion analyzer.*

Cycle	Level spacing (%)	Data bytes	Accumulation time (min) S/C track	Accumulation time (min) S/C store	Repetition time (min) S/C track	Repetition time (min) S/C store
S	10.0	3160	2.0	2.0	36	40
T	5.0	3160	2.0	2.0	4	8
HI	2.5	576	29.6	26.6	36	40
H*	2.5	5056	12.8			

* H-mode by command during track periods at requested times.

TABLE II. *Characteristics of the data cycles of the solar wind electron analyzer.*

Cycle	Number azimuth angles	Number polar angles	Number energy levels	Azimuth angle separation	Accumul. time (min)	Readout time (min) Track	Readout time (min) Store
2P	16	1	20	22.500°	2.0	0.8	1.6
2S	64	1	20	5.625°	2.0	3.1	6.3
3P	16	7	20	22.500°	2.0	5.5	10.9
3R	32	7	20	11.250°	2.0	10.9	21.8

TABLE III. *Electron experiment commandable modes for spacecraft tracking and data store times.*

Mode	Sequence	Data rate	Sequence time (min)	Cycle start times (min)* First	Second	Third
P	3P-2P-2P	Track	7.1	0	2.3	4.7
P	3P-2P-2P	Store	14.2	0	4.7	9.3
RS	3R-2S-2S	Track	17.2	0	5.7	11.3
RS	3R-2S-2S	Store	34.4	0	11.3	22.7

* Cycle accumulation times are all ~2.0 min.

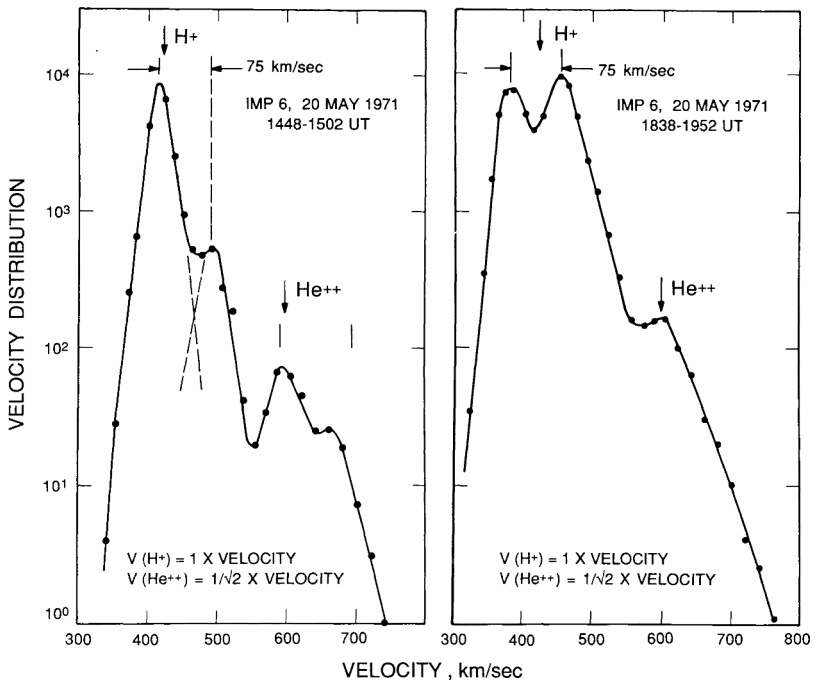

FIGURE 1. Two unusual solar wind ion spectra of the common ions, H^+ and He^{++}, obtained with IMP 6, showing two streams flowing together with different speeds.

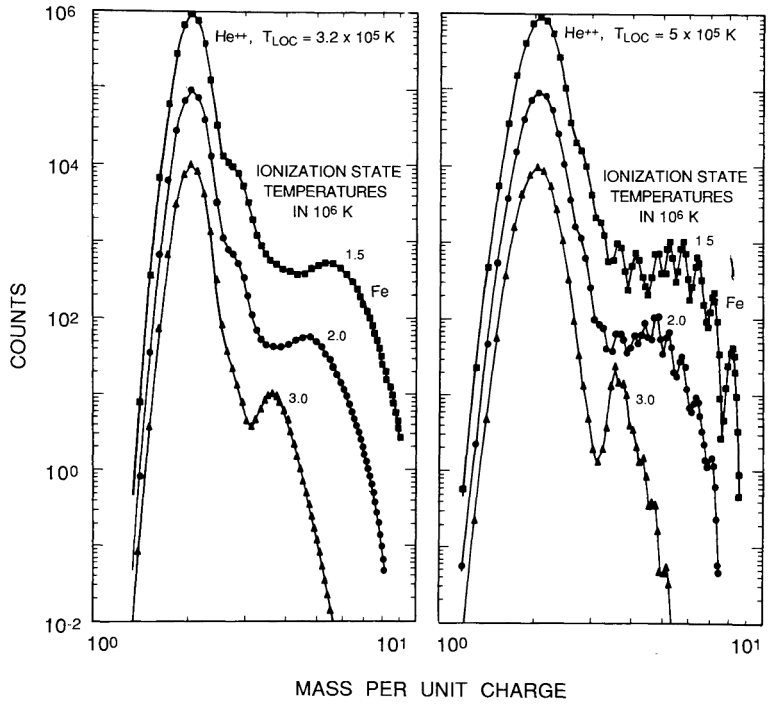

FIGURE 2. Simulated heavy ion spectra, offset from each other, showing the feasibility of determining Fe ionization state temperatures in high speed solar wind from coronal holes, using E/q measurement alone.

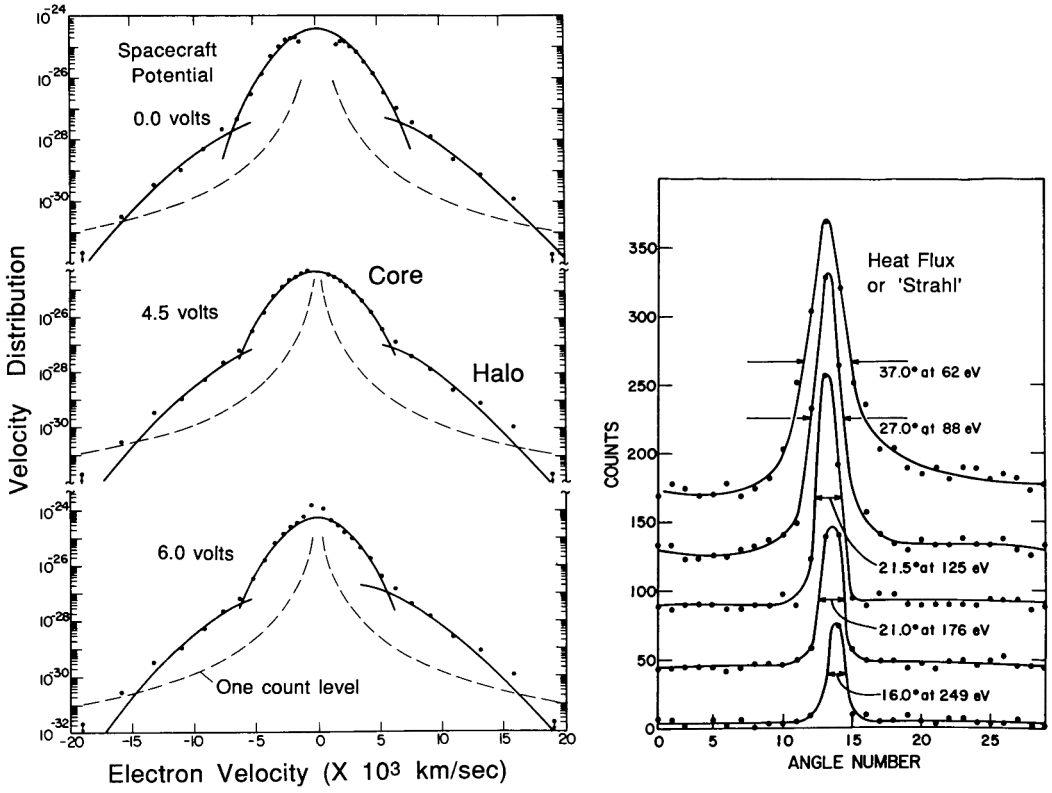

FIGURE 3. Bi-maxwellian fit to a typical solar wind electron velocity distribution (left panel), cut through along the magnetic field direction to show the existence of a low energy or 'core' component embedded in a higher energy but lower density 'halo' or 'strahl' component. A third "heat flux" component of electrons flowing out along the interplanetary field from the hot corona is illustrated on the right.

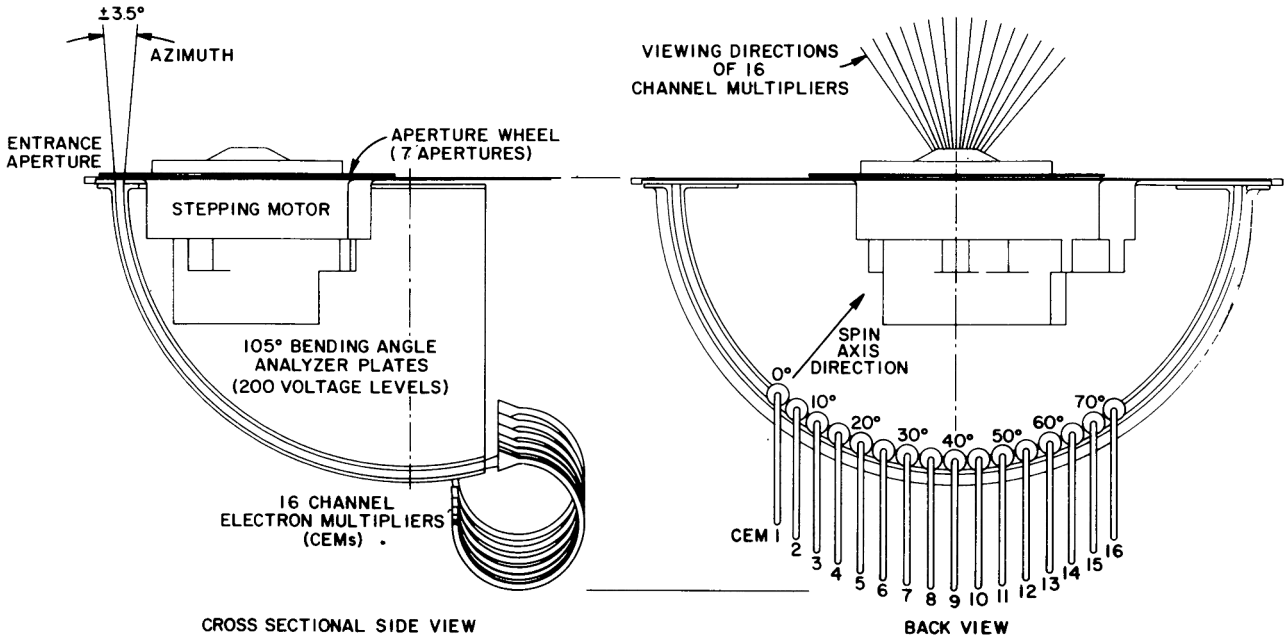

FIGURE 4. Ion optics of the SWOOPS ion experiment with a cross- sectional view on the left and a view from behind on the right. (From esa SP-1050, p.57).

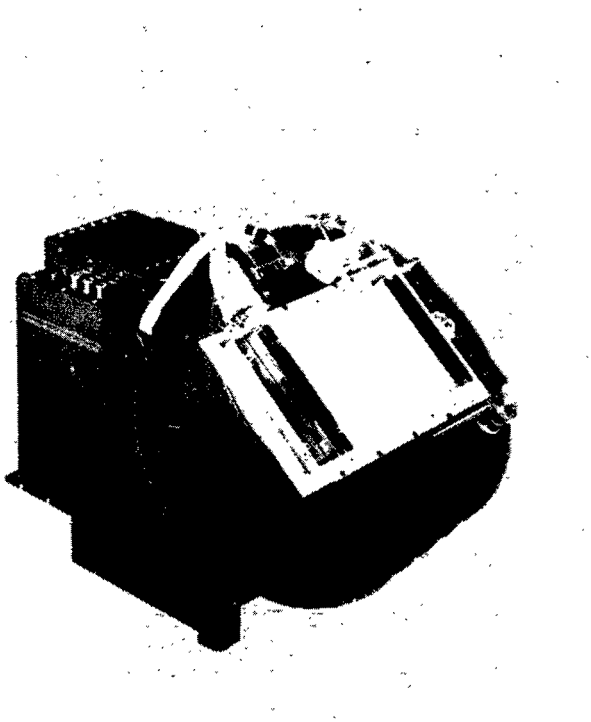

FIGURE 5. Photograph of the solar wind ion experiment package. (From esa SP-1050, p. 59).

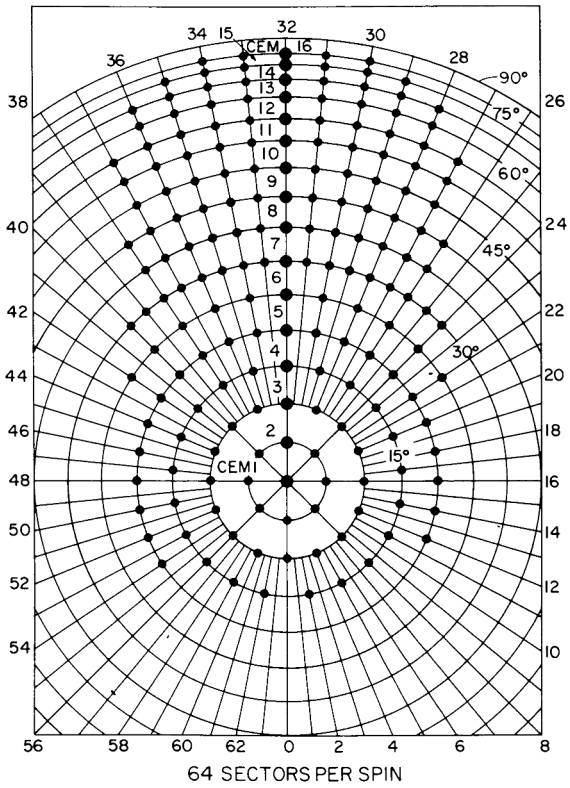

FIGURE 6. Polar representation of measurement space for solar wind ions. (From esa SP-1050, p. 60).

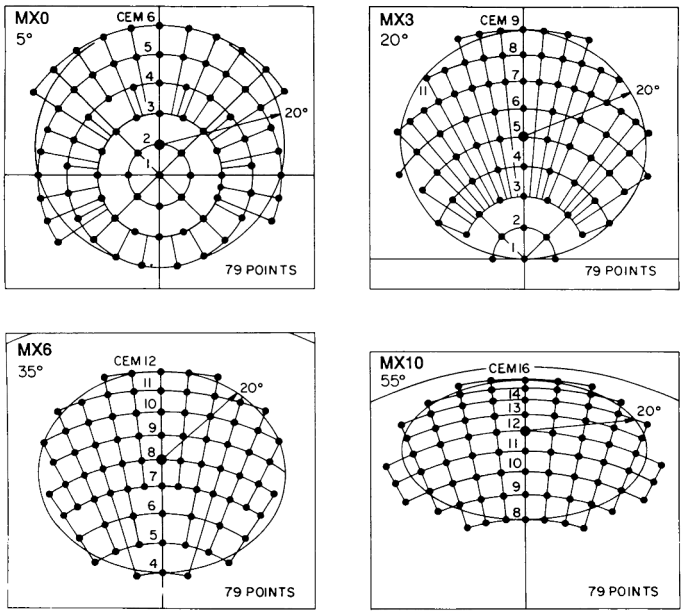

FIGURE 7. Four of the 11 measurement matrices. Each matrix, MX_n contains 79 measurement points. (From esa SP-1050, p. 61).

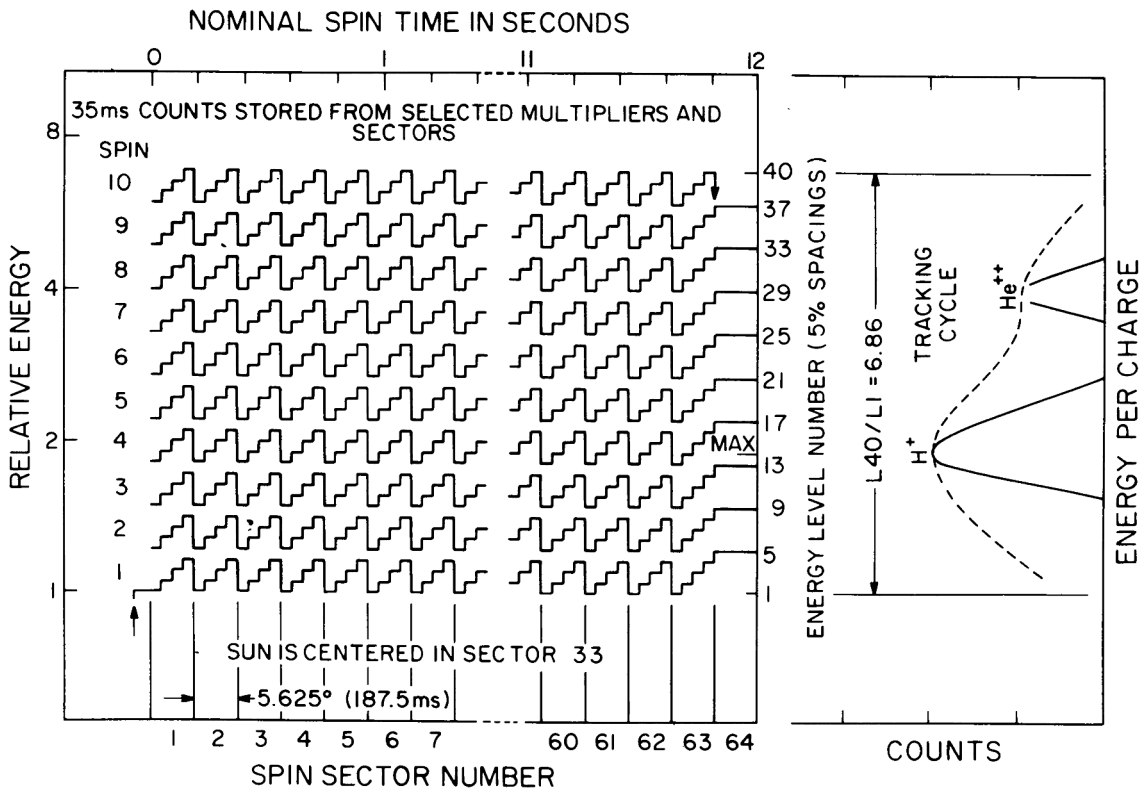

FIGURE 8. Pattern of operation of the 40 analyzer plate voltage levels during a 10-spin ion track or T- cycle. Typical H^+ - He^{++} spectra to be covered by the 40 levels are shown plotted vertically on the right side of the figure. (From esa SP-1050, p. 62).

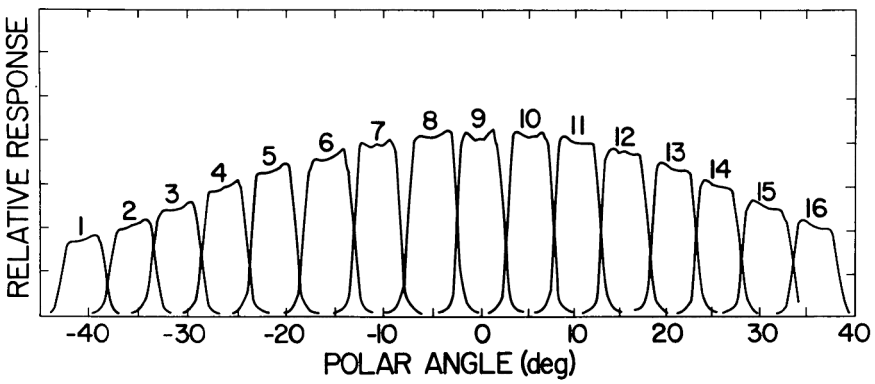

FIGURE 9. Calibrated polar acceptances of the 16 ion CEMs. (Adapted from esa SP-1050, p. 65).

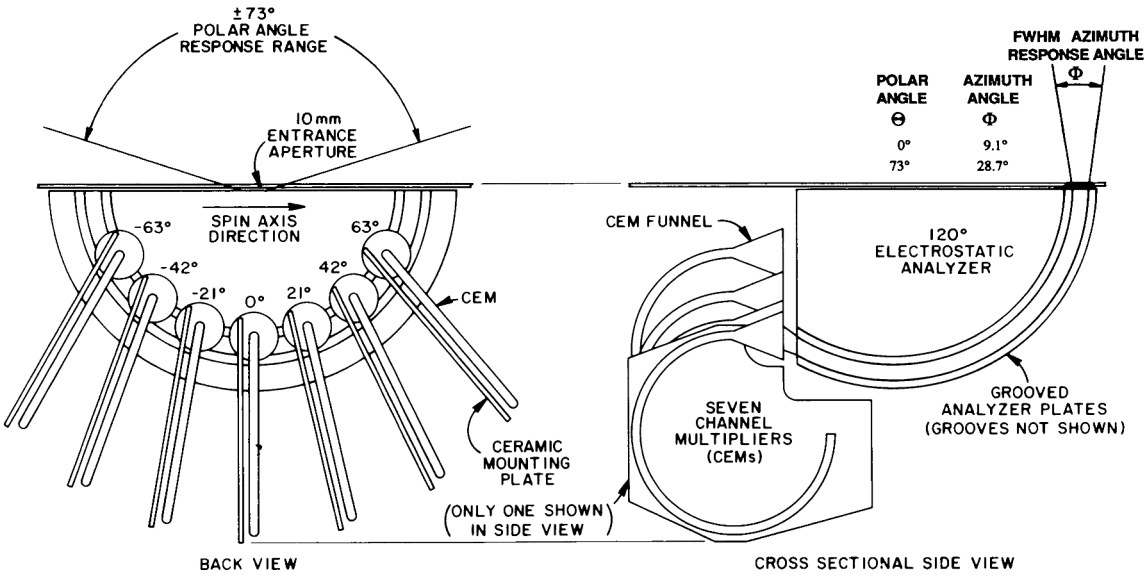

FIGURE 10. Electron optics of the SWOOPS electron analyzer. (From esa SP-1050, p. 67).

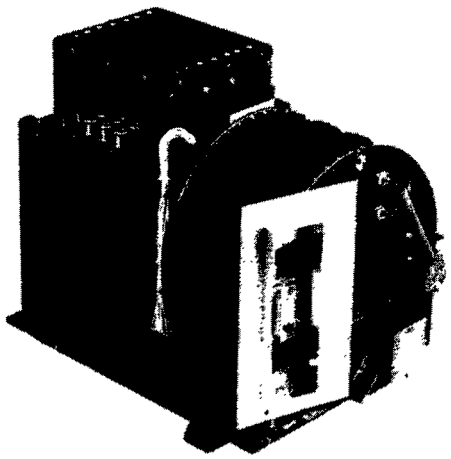

FIGURE 11. Photograph of the SWOOPS solar wind electron experiment package. (From esa SP-1050, p. 69).

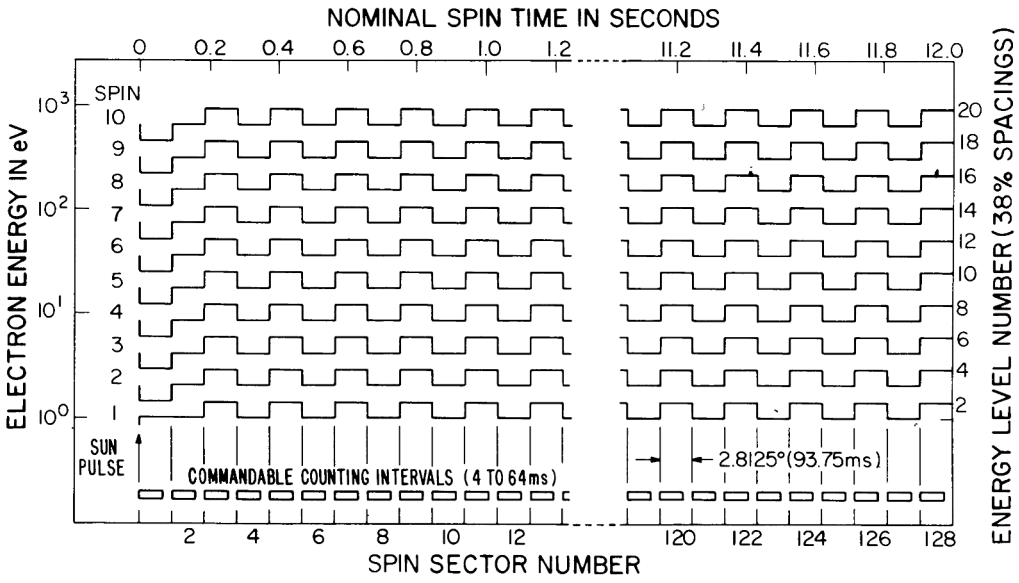

FIGURE 12. Analyzer plate voltage level operation during the 10- spin electron experiment operation cycles. (From esa SP-1050, p. 69).

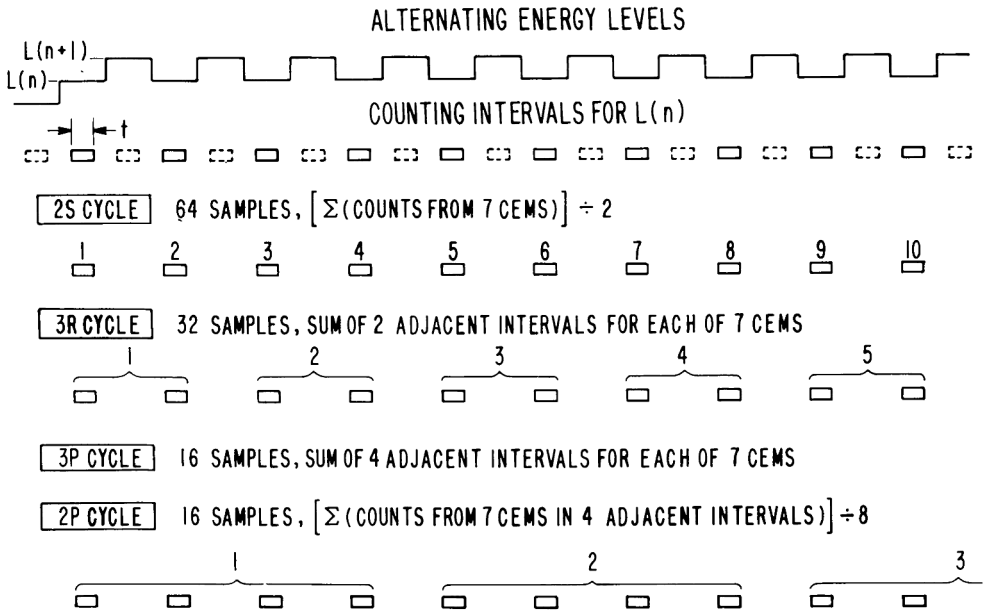

FIGURE 13. Schematic description of the four electron science data-gathering cycles: 2S, 3R, 3P, and 2P. (From esa SP-1050, p. 70).

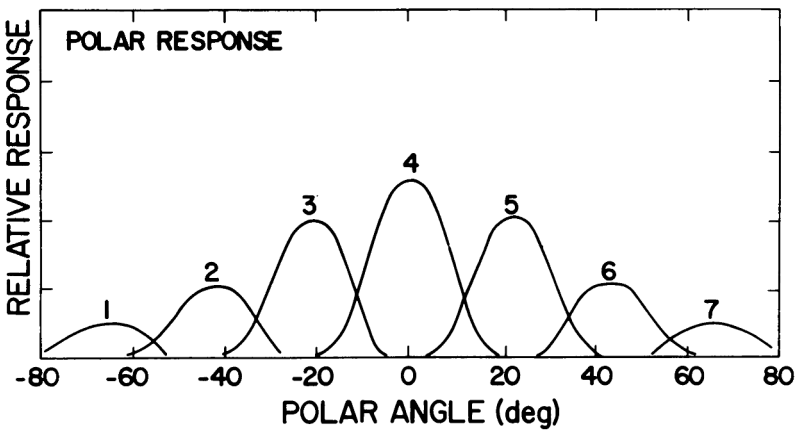

FIGURE 14. Polar angle response of the SWOOPS solar wind electron experiment. (Adapted from esa SP-1050, p. 72).

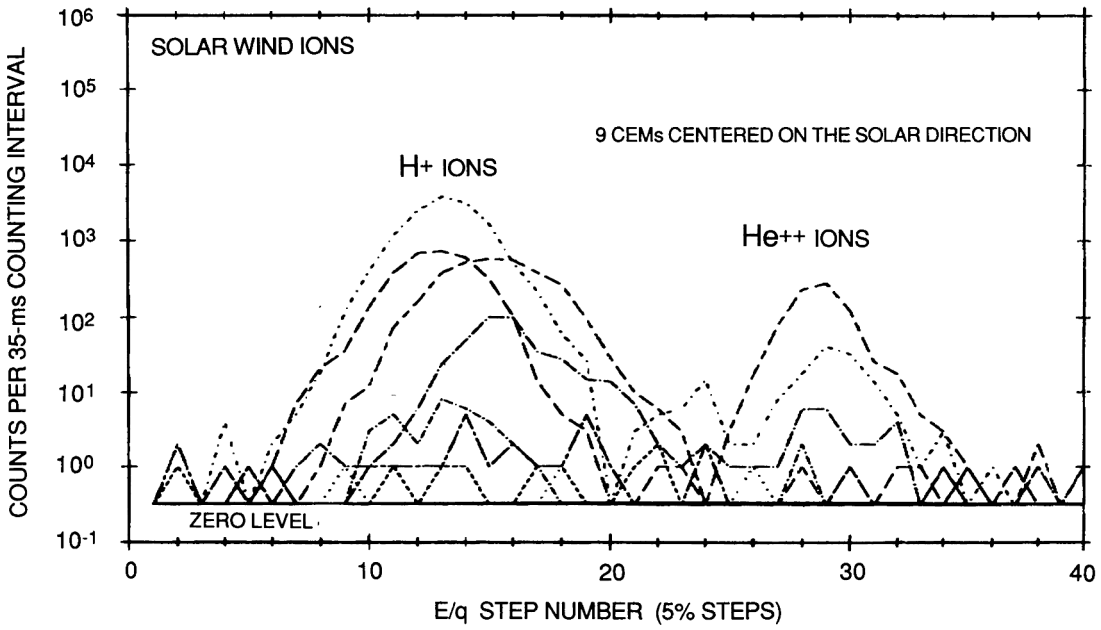

FIGURE 15. Solar wind ion E/q spectrum obtained soon after SWOOPS turn-on.

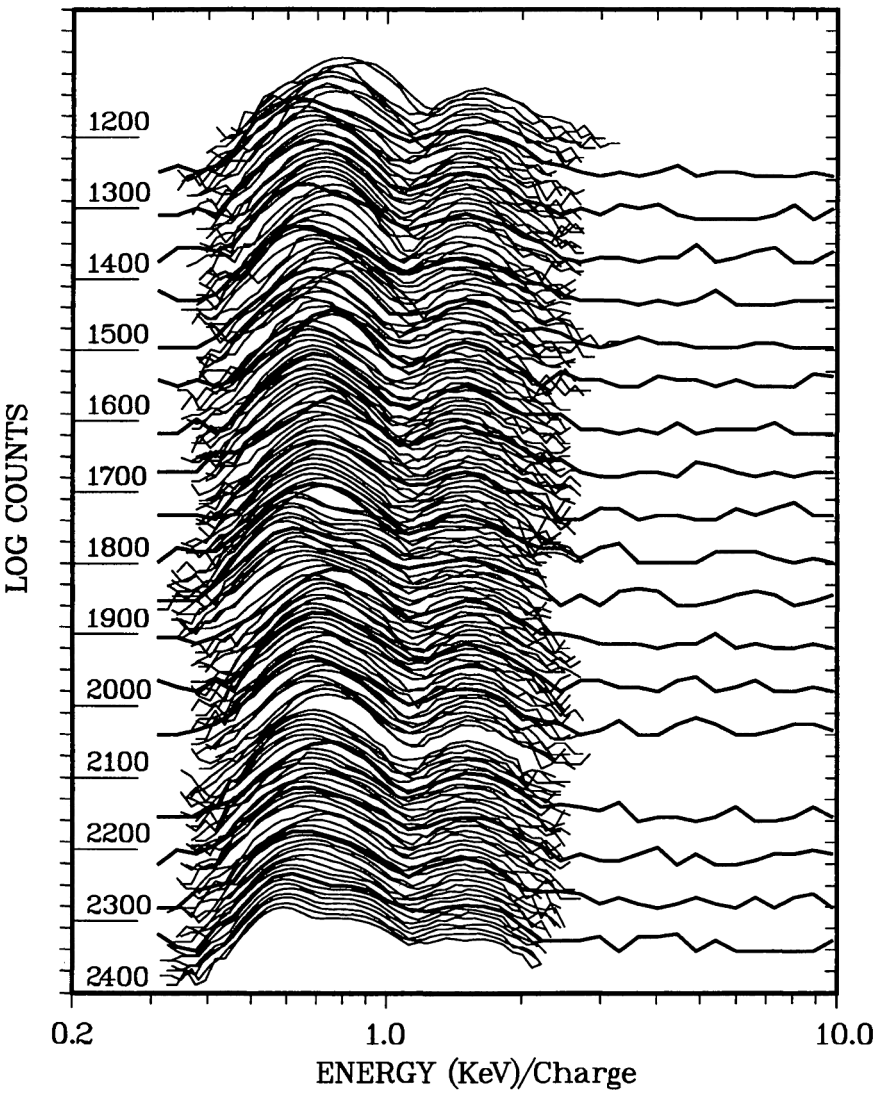

FIGURE 16. Stacked plot of E/q ion spectra obtained on 23 November 1990.

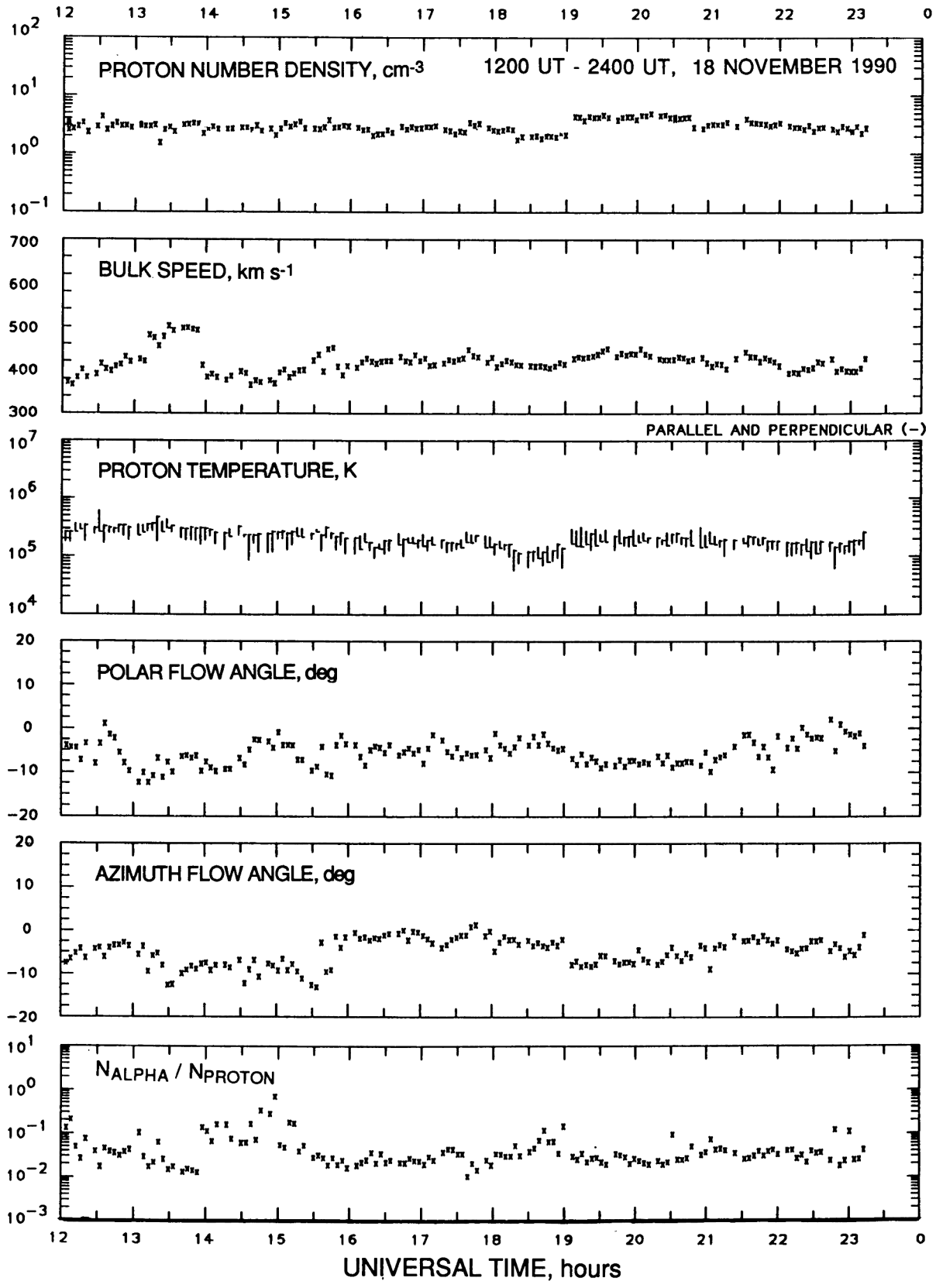

FIGURE 17. Ion moments for the second half of 18 November 1990.

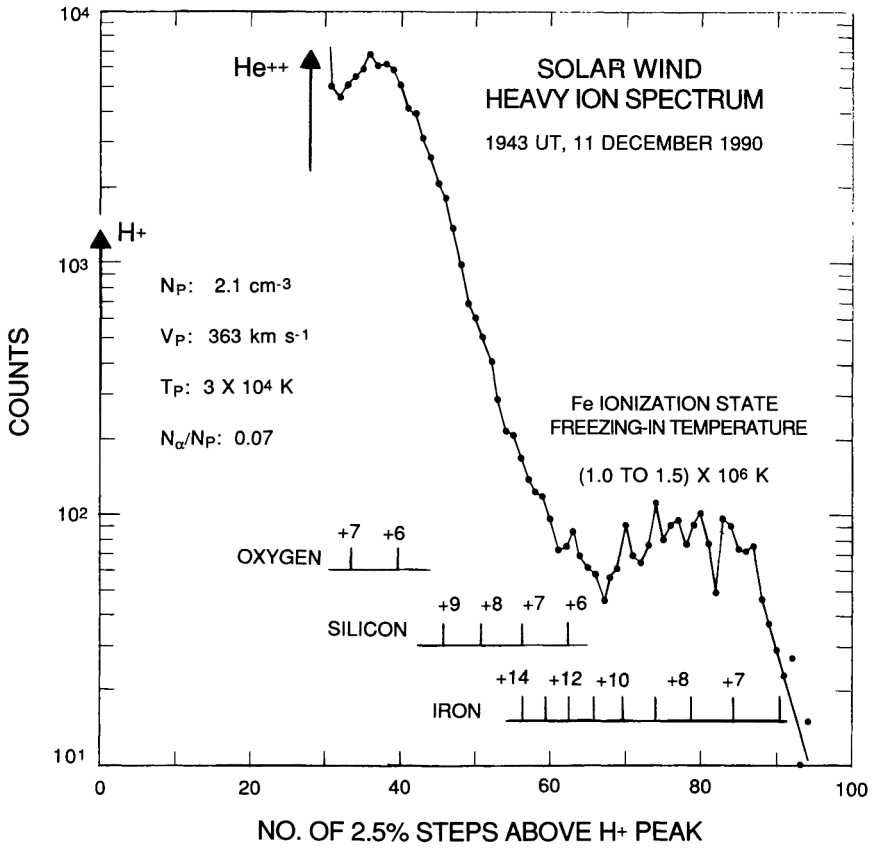

FIGURE 18. Solar wind heavy ion spectrum measured on 11 December 1990.

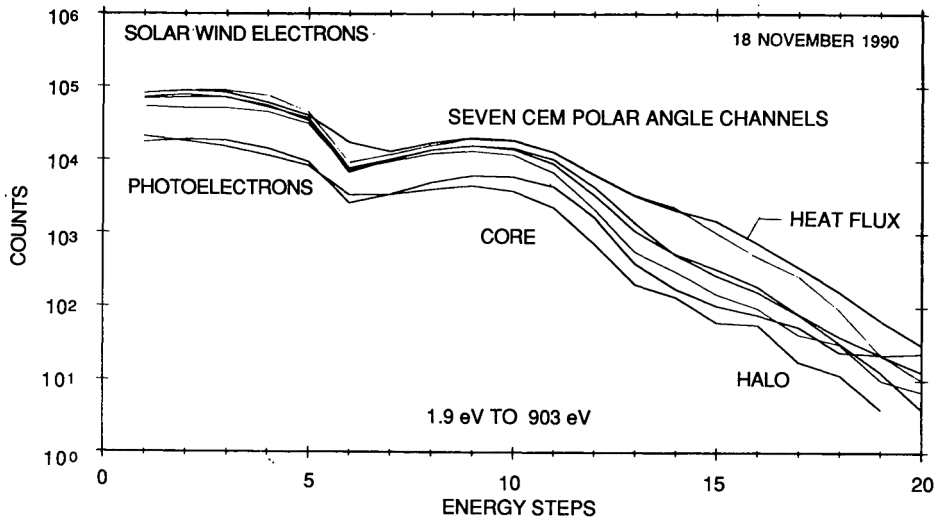

FIGURE 19. Solar wind electron spectrum obtained on 18 November 1990.

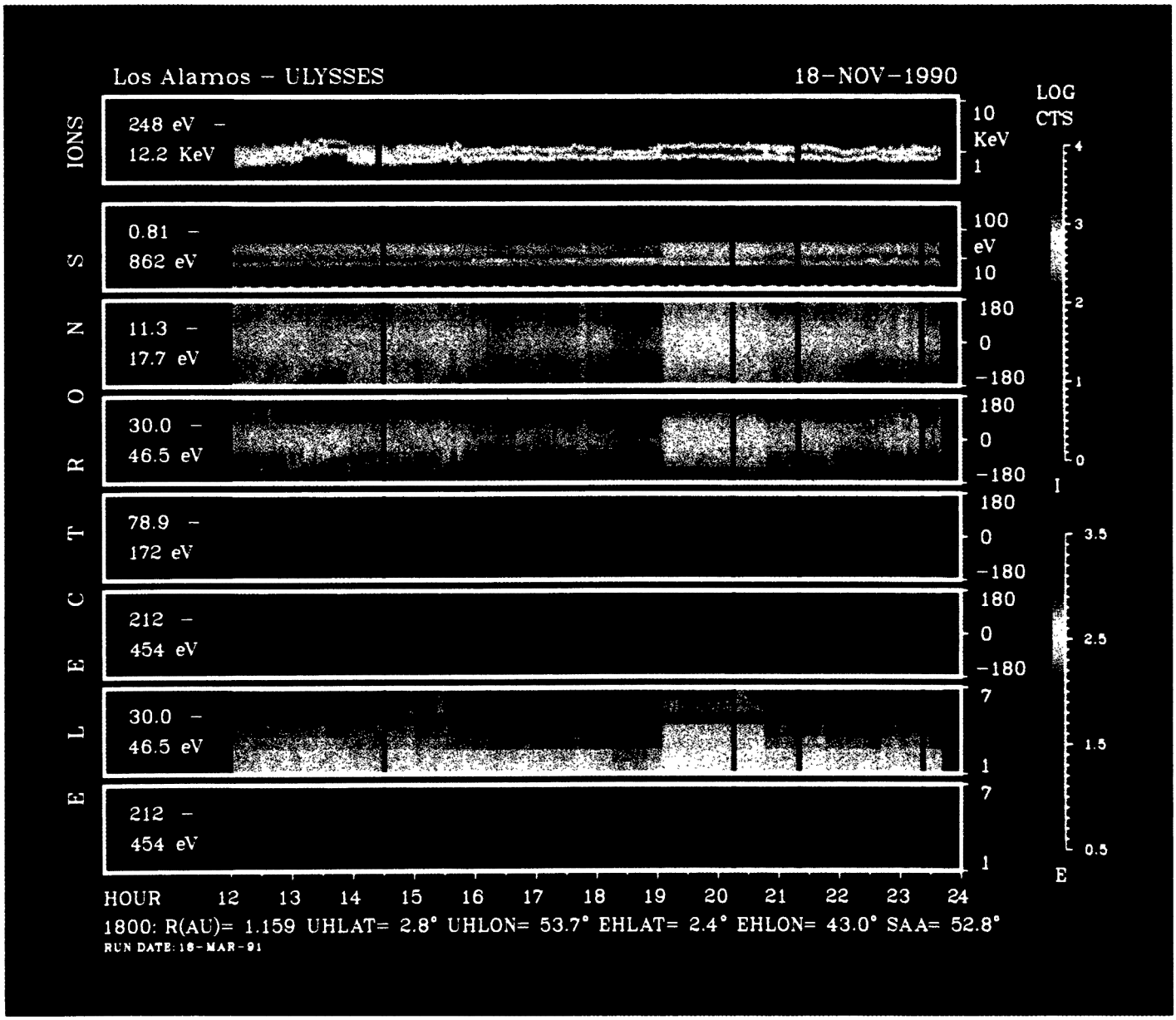

FIGURE 20. Color spectrogram of the solar wind plasma conditions on 18 November 1990.

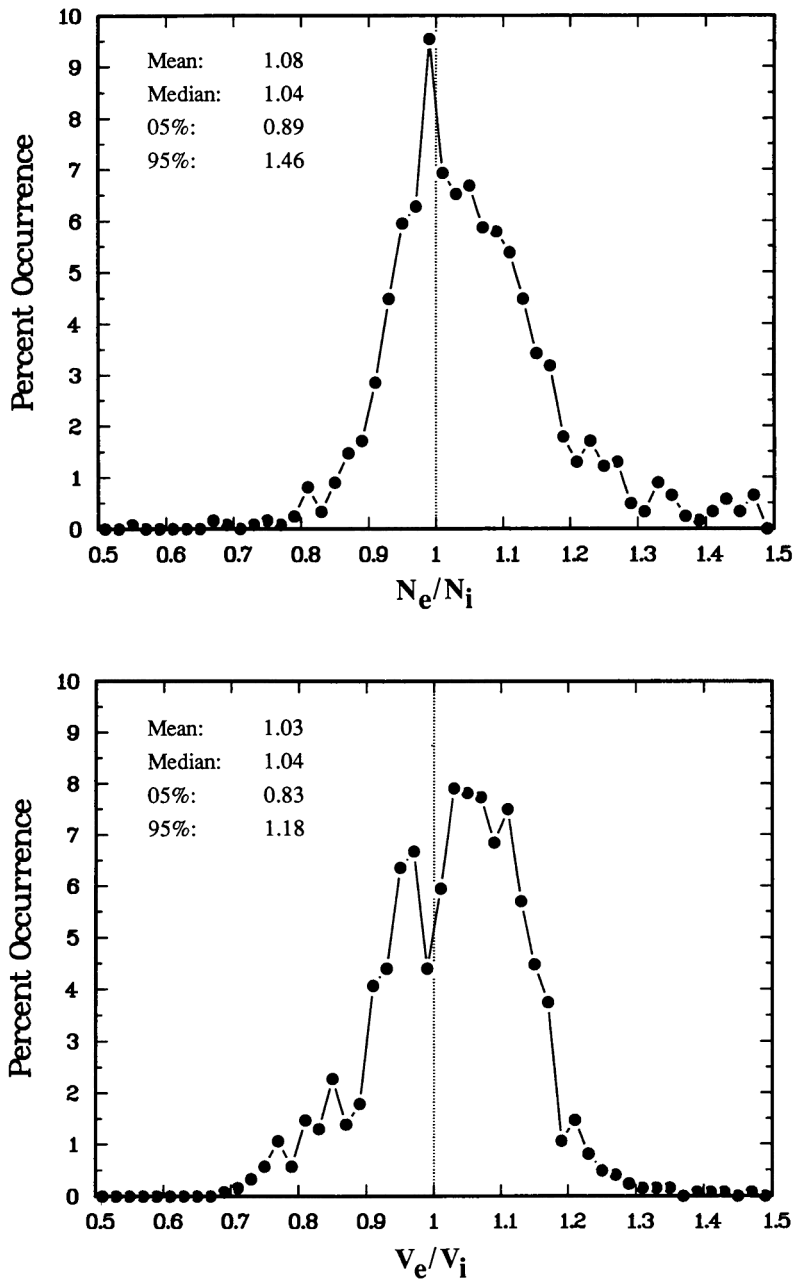

FIGURE 21. Comparison of number densities and flow speeds determined with the independent electron and ion electrostatic analyzer experiments.